Biomaterials Advances 174 (2025) 214310

Contents lists available at ScienceDirect

Biomaterials Advances

journal homepage: www.journals.elsevier.com/materials-science-and-engineering-c

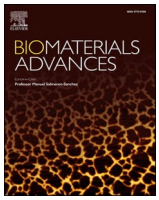

Engineering a long-lasting microvasculature *in vitro* model for traumatic injury research☆

Carla Verónica Fuenteslópez [a], Mariella Papapavlou [b], Mark S. Thompson [a], Hua Ye [a,*]

[a] Institute of Biomedical Engineering, Department of Engineering Science, University of Oxford, Old Road Campus Research Building, Roosevelt Drive, Oxford OX3 7DQ, United Kingdom
[b] Department of Materials, University of Oxford, Parks Road, Oxford OX1 3PH, United Kingdom

ARTICLE INFO

Keywords:
Microvasculature
In vitro model
Fibrinogen
Microvascular endothelial cells
3D construct
Traumatic injury

ABSTRACT

Microvascular injuries can have systemic physiological effects that exacerbate other injuries and pose a danger to life. Reliable *in vitro* microvascular models are required to enhance understanding of traumatic injuries. This research aims to develop and optimise a three-dimensional (3D) hydrogel construct for the formation and long-term stability of an *in vitro* microvascular model for trauma research.

First, we develop a 3D hydrogel scaffold using a physiologically relevant cell type to enable the formation of a durable microvascular endothelial network and validate it against the gold standard: HUVECs. Then, we explore the impact of modifying the hydrogel composition, specifically fibrinogen source and concentration, medium, and crosslinking ratio, on scaffold material properties and, consequently, the formation of endothelial networks, their architecture, and long-term integrity.

Our results demonstrate that 3D hydrogel scaffolds are crucial for maintaining network stability beyond the initial 24 h. For trauma research applications, the material properties and mechanical behaviour of the hydrogels are critical. Microrheometry revealed that fibrinogen concentration significantly influences gelation times, absorbance rate, storage modulus (G'), loss modulus (G"), and complex viscosity, while also reducing creep compliance.

Our multi-pronged approach to engineering microvasculature constructs revealed that variations in hydrogel composition, including fibrinogen concentration and source, crosslinking ratio and choice of medium, strongly affect the hydrogel material characteristics and, in turn, the resulting microvascular networks. Hydrogels made with high concentrations of human fibrinogen, a 200:10:1 crosslinking ratio, and endothelial basal medium (EBM) or EBM supplemented with VEGF performed best, demonstrating superior long-term network stability.

The microvasculature construct developed here could be used as a potential platform for studying traumatic injuries, as well as testing interventions aimed at improving recovery and mitigating damage.

1. Introduction

Traumatic injuries are a leading cause of death worldwide [1], a major contributor to long-term functional limitations [2], and can significantly diminish the quality of life for those affected. The severity and extent of soft tissue trauma often determine the outcomes of complex injuries [3]. Current understanding of tissue trauma primarily derives from clinical findings, including patient monitoring, trauma epidemiology, and clinical markers. However, trauma research requires further understanding beyond clinical symptoms and patient prognosis. Deeper insights into the mechanisms and processes underlying traumatic injuries — such as inflammatory responses and tissue regeneration — require reliable research models [4]. There are a number of factors limiting the understanding of soft tissue injuries, in particular of non-penetrating ones, including the lack of tools to evaluate the extent of the damage and the absence of appropriate models of clinical relevance [3].

Microvascular injuries resulting from trauma can have systemic physiological effects that can exacerbate other injuries and even endanger life. In non-penetrating traumatic injuries to soft tissue,

☆ This article is part of a Special issue entitled: 'Functional biopolymers' published in Biomaterials Advances.

* Corresponding author.
E-mail addresses: carla.fuenteslopez@eng.ox.ac.uk (C.V. Fuenteslópez), mark.thompson@eng.ox.ac.uk (M.S. Thompson), hua.ye@eng.ox.ac.uk (H. Ye).

https://doi.org/10.1016/j.bioadv.2025.214310
Received 31 July 2024; Received in revised form 21 February 2025; Accepted 5 April 2025
Available online 9 April 2025

microvascular perfusion failure and delayed increase in microvascular leakage [3] are often significant contributors to tissue damage.

The microcirculation is essential for maintaining systemic health, enabling adequate function and long-term tissue survival, by delivering oxygen and metabolites to tissues while removing waste products [5]. Microvascular dysfunction has been implicated in numerous diseases; both communicable as COVID-19 [6] and non-communicable as cancer [7]. Despite its importance, research into microvascular traumatic injuries is surprisingly limited [8], especially in tissues other than the brain.

Studying the immediate and short-term effects of trauma is inherently challenging. For instance, microvascular traumatic injuries remain heavily understudied [8], particularly shortly after the trauma has occurred. While *in vivo* models address some of these challenges [9,10], they are constrained by the ethical concerns associated with the unnecessary pain and stress that the models are subjected to, the physiological differences with humans (e.g., varying microvascular trauma responses between species [4]), and logistical limitations. Therefore, there is a need for reliable *in vitro* models to gain further understanding of microvascular traumatic injuries and their underlying mechanisms.

Developing such a model, however, is not straightforward. Vascularisation and microvascularisation remain major challenges in the field of tissue engineering [11,12], which also translates into limitations in applications beyond disease modelling, such as decellularisation and recellularisation of tissues and organs for transplantation [13] and the adequate function and long-term survival of implanted tissues [14]. Without a functional vasculature, engineered tissues have repeatedly failed [15] and remain limited in size due to reliance on simple diffusion for oxygenation and nutrient delivery [12,16].

A number of methods have been used to engineer microvessels. Current strategies often involve bottom-up approaches, where one or more cell lines are incorporated into a matrix [17,18]. These models can, and have been, used as platforms to study diseases, growth and remodelling dynamics [17], and other physiological processes. Cell culture models have been developed, amongst others, using bioprinting, where sacrificial inks are used to create perfusable channels [19], and microfluidic platforms, where new endothelial segments can be perfused [19]. Within these strategies, the most promising ones provide cells with a 3D environment aiming to partially mimic the extracellular matrix (ECM). Such models have been widely used for brain blood barrier [20] and tumour [21] research, and have been instrumental in advancing knowledge on the effects of matrix properties on vascularisation [17].

Human Umbilical Vein Endothelial Cells (HUVECs) are extensively used in microvascular research due to their accessibility and well-documented ability to form new vasculature [22,23]. However, they differ from microvascular endothelial cells (MVECs) [24], which are specifically found in the microvasculature. HUVEC models are well-characterised [25], widely established, and considered to be a standard model for cell-based assays [26] to study angiogenesis [23,25,27]. They are particularly prominent in tube formation assays, where they reliably form networks of tube-like structures. However, HUVEC-based networks begin to deteriorate around 18 h after seeding and completely disintegrate within 24 h [28,29], after which time, hypoxia [30] and the absence of growth factors drive apoptosis [23] and the networks disintegrate [23,31]. This short lifespan restricts their utility for longer-term research, such as research involving traumatic injury induction and evolution monitoring.

To address this limitation, it is critical to develop an *in vitro* microvasculature model that incorporates physiologically relevant microvascular cells, maintains network integrity beyond 24 h, and features a 3D structure to provide spatial cues and mechanical attachment points. Such a model would enable its use for applications in trauma research, such as the induction of traumatic injuries and facilitate monitoring of damage progression and the impact of potential interventions over time.

In this research, we address these gaps by developing and fine-tuning a 3D microvascular construct comprising a hydrogel scaffold embedded with microvascular endothelial cells. The results are structured as follows: First, we validate the suitability of our MVEC-based construct using HUVEC-based models as the benchmark. Then, we investigate how variations in hydrogel composition — specifically fibrinogen concentration and source, medium, and crosslinking ratio — affect the material properties of the scaffolds and, consequently, the formation, architecture, and longer-term stability of the resulting microvascular endothelial network. Finally, we integrate these findings to optimise the hydrogel composition and develop a long-lasting microvascular construct tailored for traumatic injury research. By focusing on a time frame of up to 14 days post-seeding, we create a platform for traumatic injury research that allows conducting further experimental work, perform additional characterisation, and accounts for the degradation time frame of the hydrogel construct itself.

2. Materials and methods

2.1. Cell culture

Human Umbilical Vein Endothelial Cells (HUVECs; ATCC) and immortalised Human Dermal Microvascular Endothelial Cells (MVECs; ATCC, CRL-3243) were cultured in T-75 and T-175 cell culture flasks (Corning Incorporated Life Sciences, USA) with Endothelial Cell Growth Medium (EGM). EGM was prepared by supplementing Endothelial Cell Basal Medium (EBM) with either SingleQuots[1] (Lonza, Walkersville, MD, USA) or Microvascular SingleQuots[2] (Lonza, Walkersville, MD, USA), respectively, and with 1% penicillin/streptomycin (Gibco Life Technologies, Grand Island, NY, USA). Cells were incubated at 37 °C and 5% CO_2, and the medium was replaced every 48–72 h, as needed. The MVEC cell line was previously immortalised via pSVT vector transfection. Cells were used for experimental work at 80% confluency and HUVECs were only used up to passage 7.

2.2. Comparing HUVECs and MVECs: morphology & cell migration

To further confirm the morphology similarities between HUVECs and MVECs, cells were cultured in their respective EGM, seeded in glass-bottom dishes (Ibidi, Germany) at a density of 3×10^5 cells/dish, and incubated for 24 h before imaging.

2.2.1. Cell migration

The collective cell migration rates [32] of HUVECs and MVECs on fibrin hydrogels were compared. Hydrogels were prepared as described in Section 2.3 using bovine fibrinogen at a concentration of 4 mg/ml and the EBM as medium. Cells were seeded on top of a hydrogel coat at a density of 2.5×10^4 cells/well (48-well plate). Once confluent, a p200 pipette tip was used to create a scratch wound across the cell sheet, forming a gap. Cells-only controls for both HUVECs and MVECs were also prepared, with nine replicates used for each experimental or control group. Cell migration was monitored for 24 h, during which the gap area was imaged at various time points and quantified using image analysis [33]. The average cell migration rates were calculated by dividing the change in gap area (final minus initial) by the time elapsed since the gap was created (Eq. (1)).

$$Migration\ Rate\ (\mu m^2/h) = \frac{Gap\ Area_{Initial}\ (\mu m^2) - Gap\ Area_{Final}\ (\mu m^2)}{t_{Initial\ -\ Final}\ (h)} \quad (1)$$

[1] FBS 2%; hydrocortisone 0.04%; hFGF-b 0.4%; VEGF 0.1%; R3-IGF-1 0.1%; ascorbic acid 0.1%; hEGF 0.1%; GA-1000 0.1%; heparin 0.1%.

[2] FBS 10%; hydrocortisone 0.04%; hFGF-b 0.4%; VEGF 0.1%; R3-IGF-1 0.1%; ascorbic acid 0.1%; hEGF 0.1%; GA-1000 0.1%

2.3. Hydrogel fabrication

Hydrogel scaffolds were fabricated and embedded with either HUVECs or MVECs to create tissue engineering constructs. Several variations of the hydrogels were explored, arising from different combinations of medium, fibrinogen concentration and source, and crosslinking ratio (Table 1). The hydrogels were prepared using fibrinogen from either bovine (MP Biomedicals, New Zealand) or human plasma (Sigma-Life Science; St Louis, MO, United States) at different concentrations (2, 4, 6, 8, 10 mg/ml) and with various media: MES/*NaCl* buffer (0.15 M *NaCl*, 2.5 mM MES in distilled water; pH 7.4); EBM; EBM supplemented with Vascular Endothelial Growth Factor (EBM + VEGF; Lonza, Walkersville, MD, USA); EBM supplemented with the full SingleQuot Kit (EGM); or Phosphate Buffered Saline (PBS; pH 7.4; Gibco, United Kingdom).

Each hydrogel was prepared from its corresponding solution. Briefly, fibrinogen at the desired concentration was dissolved in the medium and stored at 37 °C for 30 min or until fully dissolved. The solution was then filtered twice using 0.22 μm filters (Merck Millipore Ltd., Ireland) and irradiated with UV light for 20 min. Next, 100 μl of foetal bovine serum (FBS; Bioclear, United Kingdom) and cells suspended in EBM at the desired concentration were added. The solution was crosslinked with thrombin (Sigma-Aldrich, St Louis, MO, United States), previously diluted to 10 U/ml in MES/*NaCl* buffer, and a 1 M $CaCl_2$ solution in distilled water. The hydrogel solution was thoroughly mixed to ensure homogeneity before carefully casting it into the well, avoiding bubble formation and ensuring an even distribution. Finally, plates were incubated at 37 °C and 5% CO_2, to complete the gelation process.

2.4. Influence of hydrogel composition on endothelial network: architecture & integrity

To assess the impact of variations in hydrogel composition on microvascular network formation, architecture, and degradation, multiple tube formation assays were performed and characterised at various time points. HUVECs and MVECs were cultured in their respective EGM and, once confluent, seeded into a range of hydrogel scaffolds. Variations in medium, fibrinogen concentration and source, and crosslinking ratio explored are detailed in Table 1. From this point onwards, EBM was used to culture the cell-embedded constructs.

Tube formation was monitored at different time points and the network architecture was characterised using image analysis. Network characterisation of the endothelial networks included parameters such as the number of junctions (representing bifurcations), segments (elements between two junctions) and branches (elements between a junction and an extremity); the total network length given by the sum of the length of all segments, isolated elements and branches; and the branching interval, which is the mean distance separating two branches (total segments length by number of branches) [34]. A schematic of these architectural elements is presented in Fig. 1. These parameters are commonly used to characterise microvascular architecture [35], including in clinical contexts [36], as they provide insights into vessel connectivity rather than of individual vessel length and diameter, which are typically analysed through network geometry [37].

Table 1
Summary of hydrogel composition variations explored.

Medium	a) MES/*NaCl* Buffer b) Endothelial Basal Medium (EBM) c) EBM supplemented with 2% *w/v* Vascular Endothelial Growth Factor (EBM + VEGF) d) EBM supplemented with full SingleQuot Kit[2] (EGM) e) Phosphate Buffered Saline (PBS)
Fibrinogen Concentration	a) 2 mg/ml b) 4 mg/ml c) 6 mg/ml d) 8 mg/ml e) 10 mg/ml
Fibrinogen Source	a) Bovine b) Human
Crosslinking Ratio (Fibrinogen : Thrombin : $CaCl_2$)	a) 200:10:1 b) 100:10:1

2.5. Material characterisation

2.5.1. Gelation time

1 ml of each hydrogel solution were prepared and cast onto a 12-well plate. The plate was tilted periodically, and the time at which the hydrogel retained its shape was manually recorded (Fig. S 1). Five replicates were used.

2.5.2. Spectrophotometry

To gain further understanding on polymerisation dynamics, turbidity during polymerisation was measured using a spectrophotometer (WPA Lightwave II UV–Vis) at 340 nm absorbance [38–40]. Wavelengths in the 320–360 nm range are well-established for fibrin [38,41–44], with studies reporting maximal optical density differences between polymerised and non-polymerised states within this region (e.g., Montero et al., 2021). Specifically, fibrinogen emission spectra peak within this wavelength range, reaching the maximum at 344 nm [43] and 340 nm [38], which has been explicitly reported for absorbance measurements [38,40]. 600 μl of hydrogel solution were gently deposited into a quartz cuvette for spectrophotometry readings. The light absorbance of each medium was measured for zero absorbance calibration, then the absorbance of the hydrogels was measured at 1-s intervals for 5 min. Nine replicates were used.

2.5.3. Microrheology and crosslink density

To investigate energy storage and dissipation at the microscale of the different hydrogel compositions, microrheology studies were conducted using RheoLab (LS Instruments) with a multi-tau duration of 60s and echo of 30s. The device was calibrated using distilled water and the manufacturer's polystyrene solution, prior to all readings. 50 μl of a 1% solution of 1 μm polystyrene particle tracer solution (Sigma Aldrich) was added to 450 μl of each hydrogel solution, mixed, and immediately placed into a 2 mm thick glass cuvette. After allowing the mixture to gelate for 1 h (Fig. S 2), the sample was transferred to the device and equilibrated to 37 °C for 10 min before microrheology readings were performed. The polystyrene particles were stored at 4 °C when not in use. Measurements were repeated 24 h after gelation.

To complement the microrheology data, crosslink density (q; Eq. (2)) was calculated using the molecular weight of the monomer (*Mw*) and the molecular weight between crosslinks (*Mc*; Eq. (3)), with the universal gas constant (R), the absolute temperature (T), and the polymer density (d) [45].

$$q = \frac{M_w}{M_c} \tag{2}$$

$$M_c = \frac{RTd}{G'} \tag{3}$$

2.5.4. Hydrogel degradation

Hydrogel degradation profiles were analysed, focusing on the influence of medium, fibrinogen source, and concentration. Hydrogels were fabricated using fibrinogen from bovine and human plasma at different concentrations (2, 4, 6, 8, 10 mg/ml) combined with a range of media (EBM, EBM + VEGF; EGM; or PBS). 100 μl of each hydrogel solution was carefully deposited into each well (96-well plate) to avoid bubble formation. Following hydrogel casting, plates were incubated at 37 °C and 5% CO_2 for 14 days.

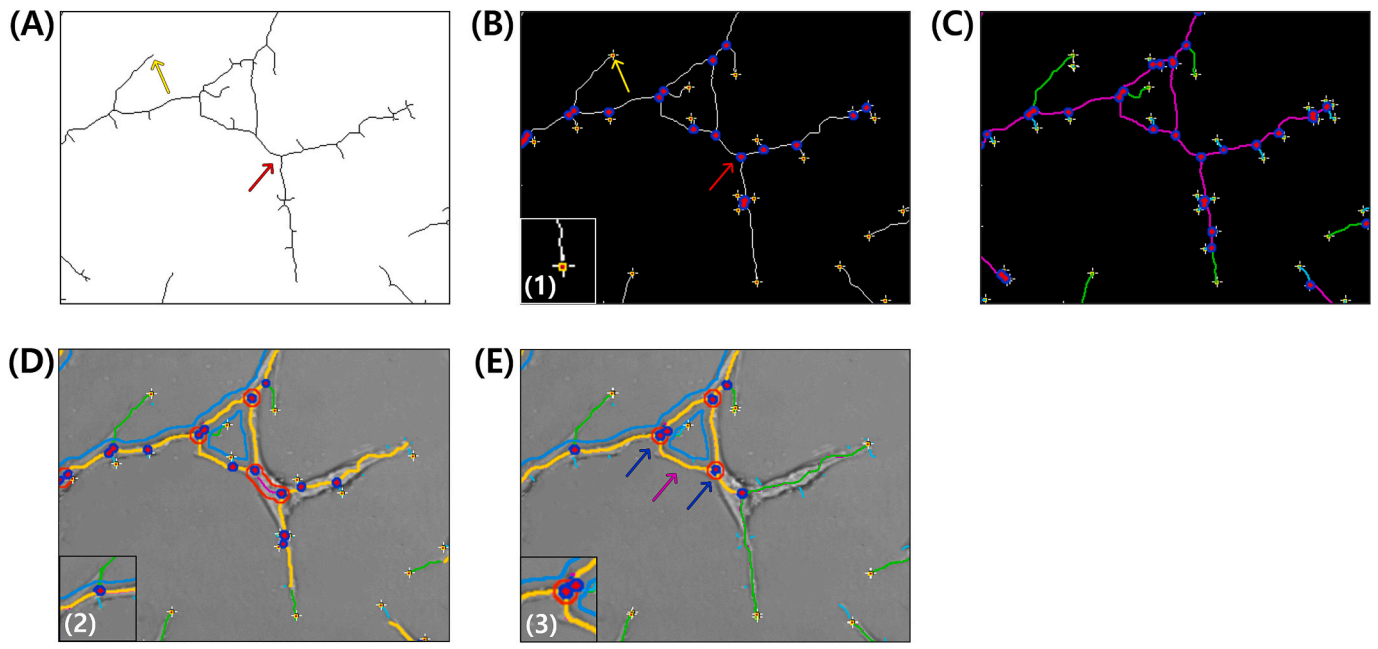

Fig. 1. Constitutive elements of the endothelial network. (A, B) Extremities (yellow arrow) are marked by red dots surrounded in yellow (shown in B1). (A, B) Nodes (red arrow) represent bifurcations and are identified as pixels that have at least three neighbours. (C, D) Twigs (cyan) are branches smaller than a defined threshold; segments (magenta) are elements between two junctions (shown in D2); and branches (green) are elements between a junction and an extremity. (E) Some segments and junctions can be further classified as master segments and master junctions, respectively. Master segments (magenta arrow) are elements located between by two junctions, neither of which is exclusively associated with a single branch. These junctions, named master junctions (blue arrows), occur where at least three master segments meet or (shown in E3) where two master junctions merge into a single unique master junction. Master junctions (blue arrows) define the boundaries of master segments (magenta arrow). Based on [34].

The mass of each hydrogel ($n = 3$) was measured on days 1, 4, 7 and 14 after casting, carefully removing the hydrogel from the well and weighing it, discarding the supernatant. After weighing, the hydrogels were returned to the well and fresh medium was added. The data was normalised to reflect the relative mass changes over time.

2.5.5. Evaluating hydrogel compositions for long-term microvascular network integrity

Insights from hydrogel composition analysis and material characterisation informed the selection of optimised hydrogel formulations for further experimental work, with a focus on long-term network durability. Additional hydrogel constructs were prepared as described in Section 2.3, and network development was routinely monitored and quantified for up to 13 days.

2.5.6. Imaging & image analysis

A widefield microscope (Nikon Widefield TiE2000, Japan), equipped with an environmental chamber for temperature and CO_2 levels control, was used for imaging. Each well was imaged in its entirety, and all the images that were not disrupted by the edge of the well were analysed using ImageJ/Fiji (version 2.14.0, National Institutes of Health, Bethesda, MD, USA) [46]. Endothelial networks were analysed using the *Angiogenesis Analyser* [34] plugin, while cell migration data was processed with the *Wound Healing Size Tool* [33]. *Z*-stack imaging was performed using a 20× objective lens. Images were captured in 1 μm steps, creating a series of optical sections through the hydrogel. Then, they were processed using ImageJ/Fiji's *Temporal-Color Code* plugin to visualise depth by assigning different colours to each slice, enabling a clearer interpretation of the 3D structure.

2.5.7. Statistical analysis and software

Data was analysed using one- or two-way analysis of variance (ANOVA), followed by Tukey's honest significant difference (HSD), Fisher's least significant difference (LSD), or Dunnett post hoc tests. p values ≤ 0.05 were considered statistically significant. Data analysis was performed using Excel 365 MSO (version 2403, Microsoft, Redmond, WA, USA) and GraphPad Prism (version 10.2.3 (403), Dotmatics, Boston, MA, USA). Unless otherwise specified, results are presented as mean values with standard deviation. Figures were created using GraphPad Prism, while the graphical abstract and the gelation process illustration (Fig. S 1) were created using BioRender.com (agreement numbers: PQ284GJ5UK & PJ284GIXSG).

3. Results & discussion

The key findings of this research include that MVECs can be used to provide a rich microvascular network that is more durable than HUVECs, the gold standard. Moreover, embedding endothelial cells in a 3D hydrogel construct enables endothelial networks that have a greater total length and are more complex, including a greater number of segments, branches and junctions. Furthermore, varying the hydrogel composition in terms of fibrinogen source and concentration, crosslinking ratio, and media has an impact on the material properties of the scaffold, network architecture and long-term network integrity. By enabling longer-term network durability, this opens avenues for further experimental work. For example, it facilitates research into microvascular network damage caused by various traumatic injuries, reducing or eliminating the need for *in vivo* models.

3.1. Comparing HUVECs and MVECs

Previously, we demonstrated that fibrin hydrogels not only support the formation of capillary-like networks of HUVECs [47] but were also the most promising polymer of the ones screened for the development of an endothelial network construct. However, macrovascular endothelial cells such as HUVECs differ from microvascular cells in several ways; for instance, types and amounts of cell adhesion molecules, prostaglandin secretory profile, and secreted proteins [24,48–50]. Moreover, MVECs

express specific proteins associated with tight junctions that are required to regulate capillary permeability [51], which is a key feature of the microvasculature.

To develop a microvasculature construct that is more physiologically relevant, we explored fibrin hydrogels for the development of a microvascular construct using MVECs. Here, HUVECs were used as the benchmark based on their extensive use in research, particularly as general models for endothelial cells in both diseased and normal conditions [22]. This comparison aimed to validate the suitability of fibrin hydrogel scaffolds for capillary-like network formation by MVECs.

Prior to the characterisation of endothelial networks created by HUVECs or MVECs, it was of interest to compare cell morphology whilst undergoing standard cell culture, as well as cell migration (Fig. 2), to validate whether MVECs could be used for the development of a microvascular construct, similarly to the well-established HUVECs, while offering advantages such as longer retention of expected morphology and cellular characteristics over multiple passages.

3.1.1. Cell morphology

As shown in Fig. 2A & B, and consistent with the literature, both cell lines exhibit an elliptical shape with sharp edges, display clear nuclei in the centre, have an abundant cytoplasm, and are arranged in a typical cobblestone arrangement [52].

3.1.2. Cell migration

Collective cell migration of HUVECs and MVECs in EBM fibrin hydrogels and cells-only controls was monitored for 24 h (Fig. 2C & D). The gap area was measured immediately after its creation and at different time points throughout the 24 h period (Fig. 2E). Using this data, the average migration rate, representing the area covered per hour, was calculated (Fig. 2F). For this calculation, the gap area at $t = 23$ h was used as the final value as the exact time of gap closure is unknown (closure occurred between t = 23 h and $t = 24$ h).

HUVECs displayed a slightly faster migration rate than MVECs, but this difference was only significant when comparing between controls or hydrogels. This observation may be associated with the faster formation and degradation of HUVEC networks compared to MVECs. Similar methodologies for evaluating cell migration using scratch assays on hydrogel coatings have been reported [53,54]. These studies often utilise natural biomaterials, as is fibrin, such as collagen [55,56] and gelatine [57]. Although differences in matrix architecture [58] and hydrogel mechanical properties [59] can influence cell migration speed, the choice of cell line plays a more critical role in determining migration rates than the properties of the scaffold, just as we observed experimentally.

3.1.3. Endothelial network development & architecture

To assess the suitability of EBM hydrogels for both cell lines, network formation and architecture were examined over time. Our results suggest that using a 3D hydrogel construct plays a key role in the network architecture, resulting in more extensive and complex endothelial networks in comparison with the controls. The importance of the hydrogel microenvironment becomes even more pronounced as time progresses, particularly from 12 h post-seeding onwards (Figs. 3, S 3 & S 4).

The results presented in Fig. 3 highlight significant differences in endothelial network characteristics between HUVECs and MVECs cultured in two hydrogel scaffolds (MES/*NaCl* and EBM) and their respective controls. These findings underscore the influence of the hydrogel microenvironment on network formation and complexity. While there are significant differences in the network architecture between the cell-embedded hydrogels and the cells-only controls in either cell line, there are no significant differences when comparing both controls or both hydrogels. This suggests that MVECs can be reliably used for the development of a microvascular model as they produce similar networks to HUVECs when embedded in the same hydrogel constructs.

Quantitative analysis revealed that the number of segments and junctions, as well as the total network length, were consistently higher in cell-embedded hydrogels compared to their respective controls at both time points. This demonstrates the ability of the hydrogels to support enhanced endothelial network formation. Notably, EBM hydrogels exhibited superior performance compared to MES/*NaCl*, particularly for HUVECs but also applicable to MVECs. This was reflected in significant increases in the number of segments and junctions, as well as a higher branching interval, indicative of a more complex, interconnected network. These differences became more pronounced over time, suggesting that EBM hydrogels promote sustained network maturation.

Both hydrogels significantly improved total network length and reduced branching intervals for MVECs relative to controls, highlighting their broader applicability for endothelial network formation. These results suggest that EBM hydrogels provide a superior microenvironment for endothelial network development, particularly for HUVECs, and offer sustained support for network maturation. Such findings are critical for advancing the use of fibrin-based hydrogels in tissue engineering and regenerative medicine, where robust and interconnected endothelial networks are essential for functional constructs.

MES/*NaCl* hydrogels (Fig. S 3) were used as the starting point for hydrogel development given that fibrin-based biomaterials often utilise this biocompatible medium [60]. This data illustrates the benefit of utilising a 3D hydrogel construct on the network architecture for both cell lines. Variations in the hydrogel medium, for instance MES/*NaCl* vs. EBM (Fig. S 4), reveal that modifying the hydrogel composition impacts endothelial network architecture.

Our results suggest that EBM hydrogels are better suited for endothelial network formation (Fig. 3), leading to more (HUVECs) or similar (MVECs) number of segments. However, differences in the number of branches were less pronounced across cell lines and scaffolds. Interestingly, we see larger variations in the branching intervals than in the other parameters. This could potentially be attributed to the addition of new branches or even the disintegration of existing network structures.

To gain deeper insights into endothelial network formation, we monitored the formation of the HUVEC and MVEC networks over 39 h using time-lapse imaging (Fig. S 5). This revealed that HUVEC networks form earlier than MVEC ones, with noticeable differences in the number of segments, branches, and junctions. While total network length also increased, the differences were not statistically significant. The hydrogel scaffolds played a key role in ensuring long-term network stability, possibly attributed to the provision of a 3D construct and mechanical support.

The ability of MVECs to form more physiologically relevant networks compared to HUVECs is further supported by studies demonstrating the expression of proteins such as claudins and occludins in MVECs, which are critical for tight junction integrity [78,79]. These proteins ensure capillary permeability control, a key feature in microvascular constructs designed for trauma research.

Over time, parameters such as the number of segments, branches, and junctions increased, while branching intervals generally decreased in hydrogels. Interestingly, cells-only controls displayed higher branching larger values at later time points, which microscopy images confirmed to be due to network fragmentation.

The use of immortalised cell lines, such as MVECs, offers significant advantages over primary cells like HUVECs, including indefinite proliferation [61], which facilitates reproducibility and reduces batch-to-batch variations. Immortalised cells retain critical biological features that are characteristic of the parent cell [62] rather than pooling cells from multiple donors, as commonly occurs with HUVECs. Therefore, MVECs appear to be more promising for developing reliable and durable microvasculature constructs, especially considering for longer term construct integrity and usability.

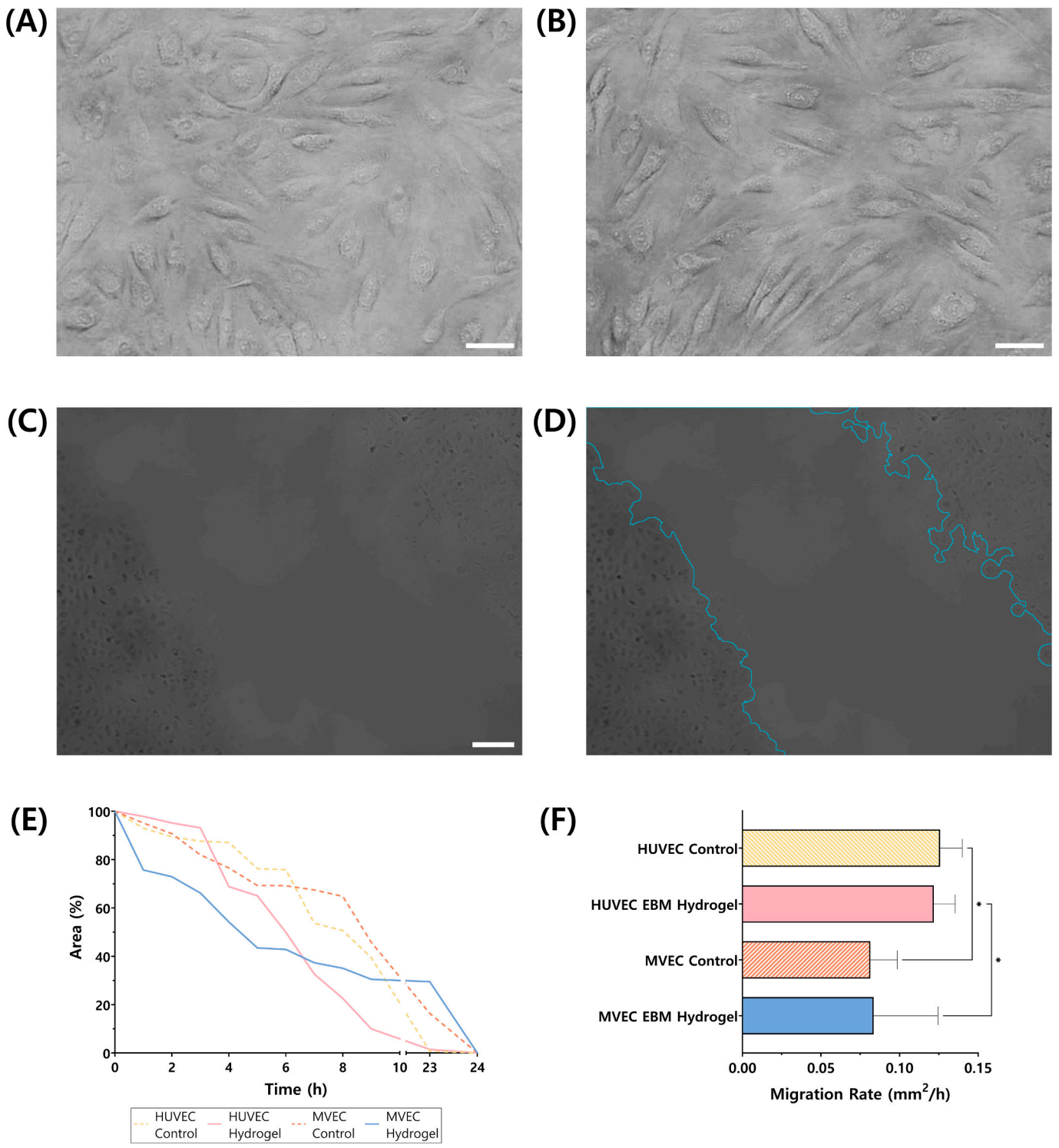

Fig. 2. Comparing human umbilical vein endothelial cells (HUVECs) and Human Dermal Microvascular Endothelial Cells (MVECs). Both (A, B) cell morphology and (D-F) cell migration were analysed. 10× microscopy images of (A) HUVECs and (B) MVECs; scale bar: 150px. Cells were cultured with their respective EGM, plated in glass-bottom dishes (cell density: 3×10^5 cells/dish), and incubated for 24 h before imaging. (C-F) Cell Migration of HUVECs and MVECs in EBM Hydrogels. (C) A gap was created using a p200 tip and imaged throughout a 24 h period. Here, the HUVEC control is shown 0.5 h after the creation of the gap. (D) Using the *Wound Healing Size Tool* [33] via ImageJ/Fiji (version 1.54f, National Institutes of Health, Bethesda, MD, USA) [46], the gap area was measured at each time point. The edge of the gap is automatically identified (blue) by the software. (E) The gap area was then plotted as the percentage of the initial gap area and, from this data (F) the average migration rate (mm^2/h) was calculated. EBM hydrogels were prepared with 4 mg/ml of fibrinogen of bovine source. HUVECs and MVECs were cultured with their respective EGM and seeded at a density of 2.5×10^4 cells/well (48-well plate). Cells-only controls were used. (One- or Two-way ANOVA/Tukey's HSD; $^*p \leq 0.05$; only statistically significant differences are shown; $n = 12$). Scale bar: 200 μm.

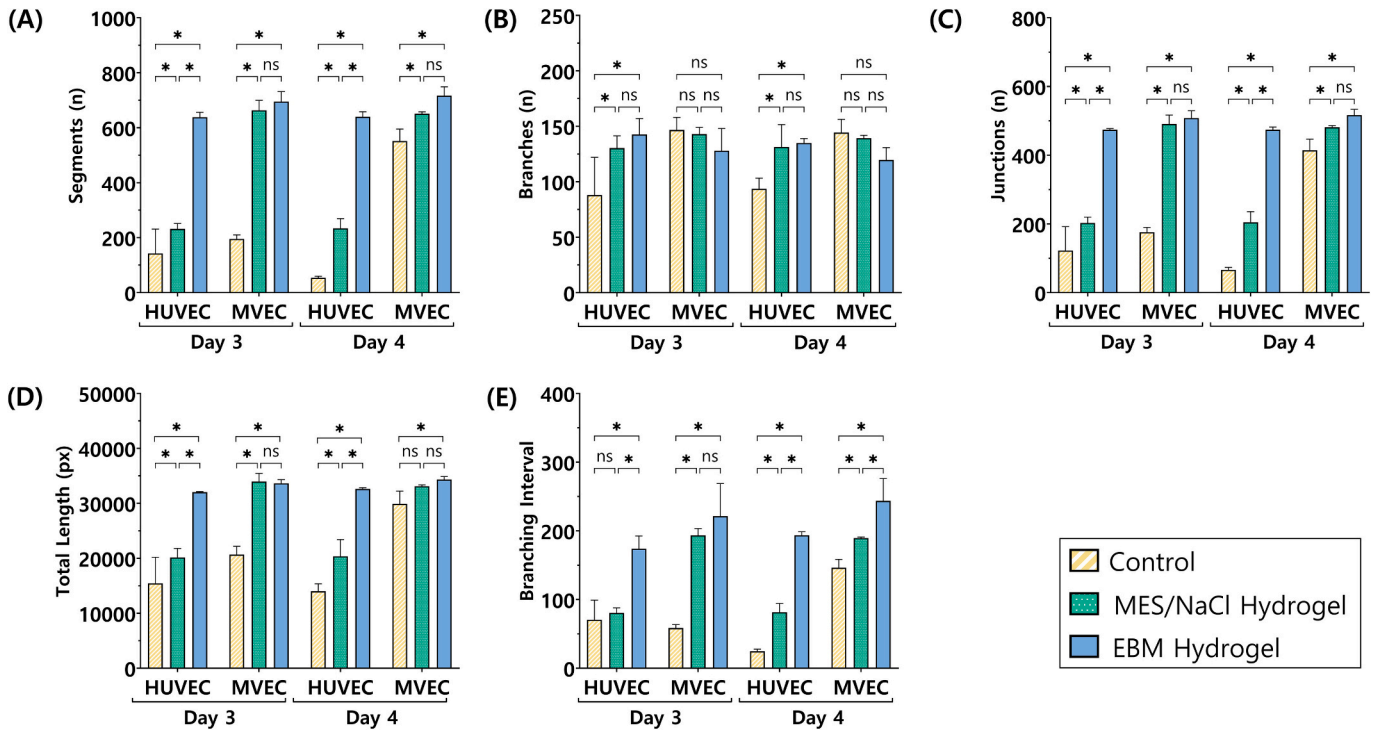

Fig. 3. Endothelial network characterisation of HUVECs or MVECs in MES/*NaCl* or EBM hydrogels using bovine fibrin hydrogel (4 mg/ml), at 3- and 4-days post-seeding. The (A) number of segments; (B) number of branches; (C) number of junctions; (D) total length; and (E) branching interval of each sample were obtained. Cell-embedded hydrogels (seeding density: 5×10^4 cells/well) were cultured with EBM in 24-well plates. Cells-only controls were used. (2-way ANOVA/Tukey's HSD; $^*p \leq 0.05$, ns: not statistically significant; $n = 3$).

3.2. 3D hydrogel constructs with MVECs enable successful endothelial network formation

The 3D hydrogel constructs developed in this research effectively facilitated the formation of endothelial networks (Fig. 4A) using both HUVECs and MVECs. Modifications to the hydrogel composition influenced the network's architecture and durability, revealing that specific formulations are more suitable for microvasculature formation. The HUVEC and MVEC networks were characterised by performing image analysis (Fig. 4B-G). This data was used to evaluate the impact of modifying the hydrogel composition (medium, fibrinogen concentration and source, and crosslinking ratio) on the formation and evolution of the endothelial networks.

To confirm the three-dimensional nature of the construct, z-stack imaging illustrated the spatial arrangement of endothelial cells embedded within the matrix, rather than on the surface of the hydrogel. MVECs are distributed throughout the hydrogel scaffold, highlighting the spatial complexity and physiological relevance of the construct (Fig. S 6). These findings underscore the ability of fibrin hydrogels to support the development of intricate, 3D microvascular networks.

The development of a stable 3D microvascular network in the hydrogel scaffold is consistent with findings that emphasise the importance of 3D matrices in recapitulating physiological microenvironments [80,81]. The interplay between the fibrin hydrogel's mechanical properties and cellular behaviour aligns with prior studies highlighting the role of ECM mimetics in supporting endothelial morphogenesis [82].

From the parameters used to quantify the microvasculature architecture (Fig. 1), the most important one would be the total network length as is the most critical indicator of an extensive network. While a high number of junctions may suggest a more complex network, this figure should always be evaluated alongside the number of segments and branches. As for the branching interval, this provides insights into how the network splits at every junction; therefore, more complex networks where multiple branches split from every segment could be more easily identified.

3.3. Influence of hydrogel composition on endothelial network: architecture & integrity

Having validated the use of MVECs for the development of the construct, it was necessary to optimise the hydrogel composition. To this end, the fibrinogen concentration, medium, and crosslinking ratio were modified to evaluate their impact on network formation and architecture.

3.3.1. Impact of variations in fibrinogen concentration and medium

The influence of fibrinogen concentration and medium on the development of a microvascular network was explored using a range of fibrinogen concentrations in combination with three medium variations: EBM, EBM + VEGF and EGM (Figs. 5 & S 7). Higher fibrinogen concentrations (6, 8 and 10 mg/ml) across all media variations resulted in longer networks compared to the controls, particularly at later time points. At lower concentrations, EBM hydrogels produced networks comparable to controls, with the 4 mg/ml concentration hydrogels contributing to slightly lengthier networks at 24 h.

All but two fibrinogen concentrations and the control have a similar total network length across the three media at 24 h. On the other hand, both 4 and 6 mg/ml display the largest variations between media and time points. This suggests that the hydrogel scaffolds play a greater role in the later stages of network formation than in the first few hours. Finally, as expected, there are significant increases between 2 h and 24 h across all variations. This further validates the growth of the microvascular network over time, which was also observed in preliminary experimental work.

Network characterisation (Fig. 5) revealed an increase in the number of segments, branches, and junctions over time, with most hydrogel formulations outperforming controls. This further supports the postulation that fibrin hydrogels are suitable for endothelial network

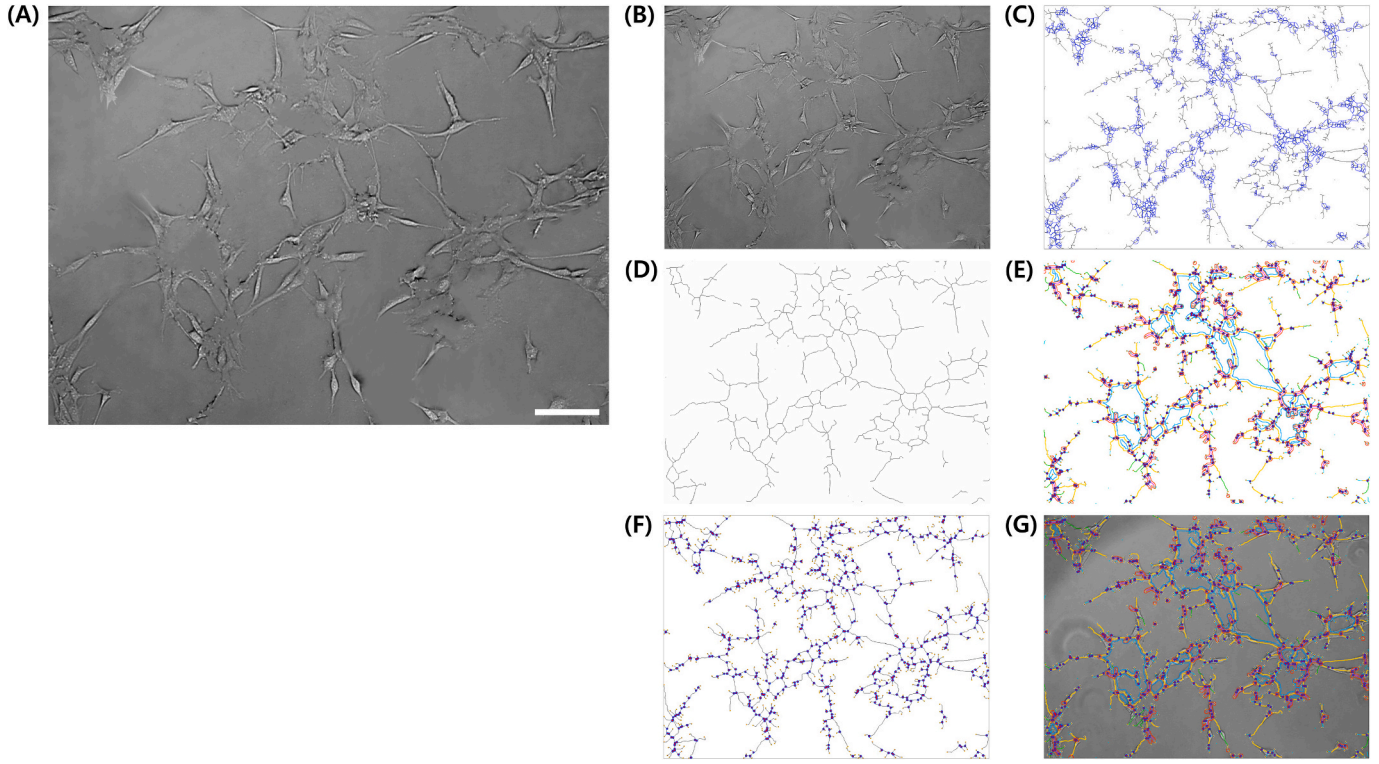

Fig. 4. Characterisation of endothelial networks. (A) Representative image depicting endothelial network formation. Here, an MVEC network in an EBM hydrogel with fibrinogen from human plasma at a concentration of 8 mg/ml and a 200:10:1 fibrinogen : thrombin : $CaCl_2$ crosslinking ratio, imaged 7 days post seeding, is shown. Cell seeding density: 2×10^4 cells/well (96-well plate). (B-G) Network characterisation was performed via image analysis, depicting the various steps involved: (A) the original microscopy image with a 100 μm scale bar; (B) the markup of the network tree on the original image; (C) the binary tree image indicating the artefactual loops (blue) to be removed; (D) the resulting master binary tree; (E) the analysis of the binary tree depicting the detected vectorised elements: extremities (red dots with yellow border), branches (green), segments (magenta), twigs (light blue), junctions (red dots with blue border), and segments (yellow); (F) extremities (red dots with yellow border) and junctions (red dots with blue border) indicated on the binary tree; and (G) the detected vectorised objects on the original image. The scale bar was removed during the image analysis process to prevent its inclusion in the network analysis. Images were analysed using ImageJ/Fiji (version 1.54f, National Institutes of Health, Bethesda, MD, USA) [46] and the *Angiogenesis Analyser* [34] plugin.

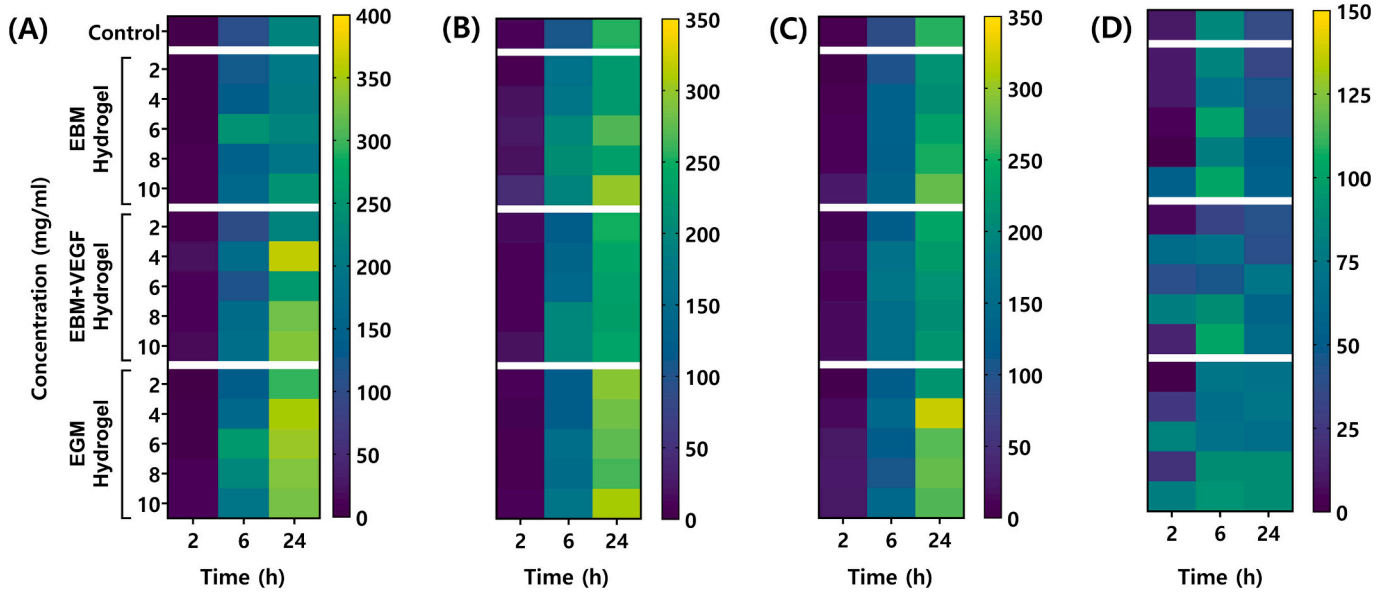

Fig. 5. Impact of variations in fibrinogen concentration and medium on microvascular endothelial network architecture, showing MVEC network characterisation by fibrinogen concentration and medium at 2, 6 and 24 h. The number of (A) segments, (B) branches, (C) junctions, and the (D) branching interval were quantified. Hydrogels were created with bovine fibrinogen. MVECs were cultured with EGM and seeded at a density of 2.5×10^4 cells/well (48-well plate). Cells-only controls were used. (ANOVA/Tukey's HSD; $n = 3$).

development. At 24 h, EBM hydrogels are associated with more segments, branches and junctions than the control, except for the 2 mg/ml concentration which displays a similar architecture to the networks of the controls. EBM + VEGF hydrogels consistently displayed more segments than controls. On the other hand, the branching interval does not exhibit discernible patterns across time points or hydrogel compositions. This could potentially be attributed to either further development of the network or its fragmentation, making this parameter less reliable for identifying optimal hydrogel compositions.

Combining total network length with architectural metrics suggests that higher fibrinogen concentrations across all three media enable the formation of larger networks. The observed improvements in network formation with higher fibrinogen concentrations may be attributed to enhanced matrix stiffness [83], which impacts endothelial cell self-organisation [84], vascular integrity [85], and vessel permeability [86]. Furthermore, increased matrix stiffness has been shown to promote endothelial tubulogenesis and network complexity. This is particularly relevant in trauma research, where matrix properties can influence angiogenic responses during wound healing and regeneration. Considering that the fibrinogen concentration of 4 mg/ml delivers promising results at the later time points, it would be interesting to explore a slightly higher concentration to determine whether 4 mg/ml is the lowest threshold enabling a more complex capillary-like network.

3.3.2. *Impact of variations in crosslinking ratio*

Two crosslinking ratios of fibrin, thrombin and $CaCl_2$ (200:10:1 and 100:10:1) were selected based on the results of the evaluation of hydrogel consistency and shape retention twelve days after casting and 1 h after demoulding (Supplementary Materials A 1), as they exhibited good shape retention and consistency. These ratios were tested to evaluate their impact on the development of capillary-like networks formed by HUVECs and MVECs. The total length of the resulting networks was quantified hourly from 0.5 h after seeding hourly, for 4 h (Figs. 6 & S 8). Crosslinking ratios play a key role not only in network development and integrity, but also in hydrogel consistency and scaffold shape retention. Crosslinking ratios have a greater impact on hydrogel consistency than fibrinogen concentration or the selection of medium.

Our results also revealed that using fibrinogen 20× or 10× relative to thrombin improves scaffold shape retention. Networks formed in 200:10:1 hydrogels exhibited steady growth over time (Fig. S 9), outperforming the 100:10:1 ratio in supporting longer and more stable networks. This ratio also improved scaffold shape retention and consistency, critical factors for long-term network durability. Interestingly, there seem to be two clusters at the earliest period: (1) the EBM cells-only control and the two highest fibrinogen concentrations, and (2) the cells in EGM control with the two lower concentrations. There is also a change from 5.5 h onwards, where the total network length of the 10 mg/ml concentration significantly increases. We can also observe notable increases in the remaining concentrations within the time frame of 6.5 to 9.5 h.

MVEC networks display a less defined pattern, particularly within the initial 18 h, which represents the primary phase of network growth, as shown in previous experimental work. By the end of this period, all hydrogel compositions with a 200:10:1 ratio, as well as most (except for

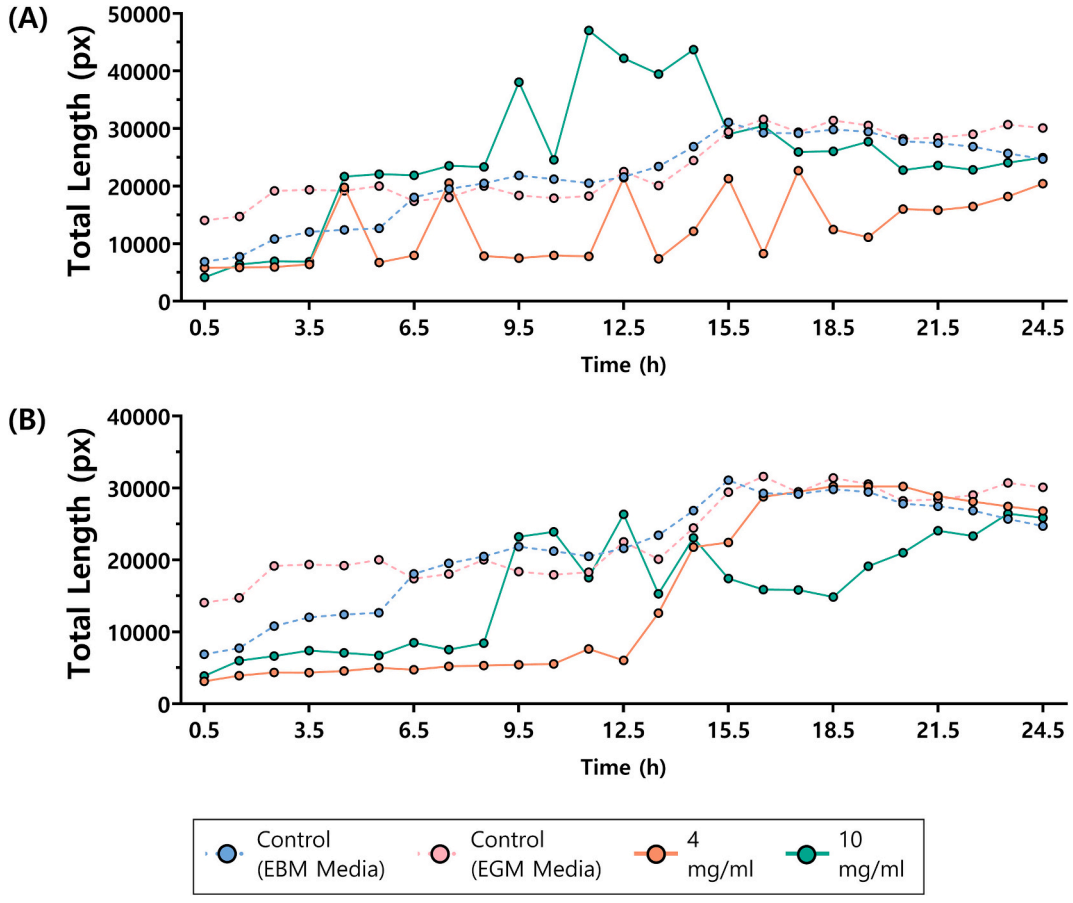

Fig. 6. Impact of Variations in Crosslinking Ratio on Microvascular Endothelial Network Architecture, displaying total MVEC network length by fibrinogen : thrombin : $CaCl_2$ crosslinking ratio, quantified every hour during a 24.5 h period. Two crosslinking ratios were explored: (A) 200:10:1 and (B) 100:10:1. Hydrogels were created using fibrinogen from human serum at different concentrations, paired with EBM as medium. MVECs were cultured with EGM and seeded at a density of 2×10^4 cells/well (96-well plate). Two cells-only controls, in EBM and EGM, were used. Here, the controls and the 4 and 10 mg/ml concentrations are shown. (ANOVA/Tukey's HSD; $p \leq 0.05$; $n = 6$).

8 and 10 mg/ml) of those with a 100:10:1 crosslinking ratio, reach a total network length in the 20,000–40,000 pixels range. Similar results are obtained when quantifying HUVEC networks, further reinforcing the suitability of the MVEC line for endothelial research.

However, it is noteworthy that despite control networks having a total length in the higher end of the range, they become extremely fragmented by the end of the period, unlike the networks embedded within 3D hydrogel constructs. This highlights the critical role of 3D scaffolds in maintaining long term network integrity. Relying solely on total network length to determine the optimal hydrogel composition has limitations. Additional insights should be derived from other parameters used to characterise the network architecture, which will be addressed in future work. Further work exploring particular pairings of crosslinking ratios and media will enable further refinement of the hydrogel composition.

3.3.3. Impact of variations in medium

Having refined the fibrinogen concentration (6, 8 & 10 mg/ml), the next step was to investigate the optimal pairings with different crosslinking ratios (100:10:1 or 200:10:1) and media (EBM, EBM + VEGF, or PBS). Over a 24 h period, the number of segments and total network length (Figs. 7 & S 10) were quantified.

EBM hydrogels are associated with a lower number of segments than their EBM + VEGF and PBS counterparts, but this was not statistically significant. This trend was particularly noticeable in higher fibrinogen concentrations and, even more so, in the 200:10:1 crosslinking ratio. Within the same medium, there are no significant differences between crosslinking ratios, although the data distribution appeared to be slightly higher for the 200:10:1 ratio. The addition of VEGF to the medium did not consistently yield significant improvements in network stability, suggesting that EBM may be preferable for simplicity and reproducibility.

Within the same hydrogel composition, the number of segments remains relatively stable, except at the 24 h time point, where a decrease was observed in all hydrogel formulations. This could potentially be attributed to either the growth of each individual segment or to partial network disintegration.

In terms of total network length, EBM hydrogels displayed less variation across ratios and fibrinogen concentrations compared to EBM + VEGF and PBS hydrogels. The 8 mg/ml concentration in both ratios showed an interesting pattern, forming the largest network in the EBM group at most time points, but with a noticeable decrease at 24 h. A similar pattern was observed in the 10 mg/ml EBM + VEGF hydrogel and four of the PBS hydrogels (8 and 10 mg/ml for both ratios).

Interestingly, lower concentrations of 100:10:1 EBM + VEGF hydrogels exhibited an interesting progression, with total network length decreasing up to 5.5 h, followed by a steady increase until 24 h. The control also exhibits a different pattern, remaining relatively stable throughout the entire period.

3.4. Material characterisation

Material characterisation provided insights into the impact of hydrogel composition on polymerisation dynamics and mechanical properties. This approach was conducted to better understand how hydrogel composition influences microvascular network formation and integrity, as well as to allow the fine tuning of the scaffold to better replicate tissue-specific microenvironments. This included analysing gelation time, spectrophotometry, microrheology (Fig. 8) and hydrogel degradation (Fig. 9). In addition to deepening our understanding of how modifications to the hydrogel composition affect its material properties, this approach could enable fine-tuning of the construct to better replicate specific tissues. For example, it could be tailored to simulate soft tissues like skeletal muscle, creating a more relevant and accurate model.

3.4.1. Gelation time

Investigating the role played by gelation time is relevant for tissue engineering constructs given its impact on the overall structural and functional properties, mechanical stability [63], cell viability [64], and

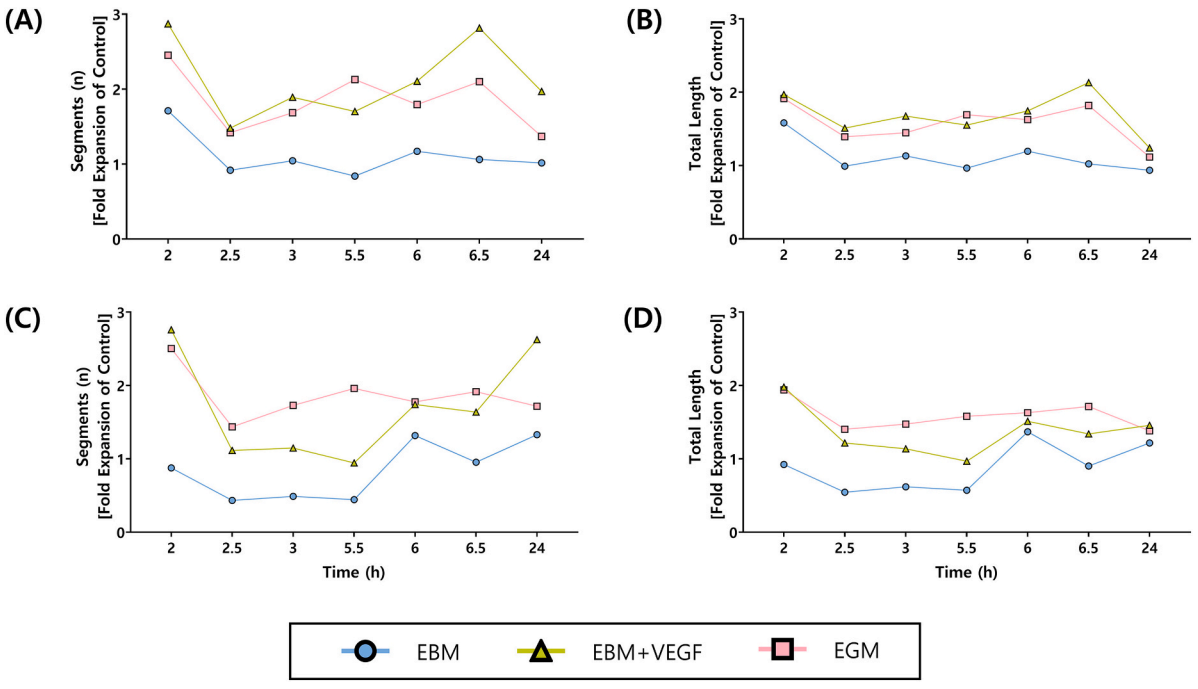

Fig. 7. Impact of variations in medium and crosslinking ratio on microvascular endothelial network architecture. (A, C) Number of segments and (B, D) total MVEC network length by medium and crosslinking ratio (fibrinogen : thrombin : $CaCl_2$) during a 24 h period, as a fold expansion of their respective controls. Hydrogels were created using fibrinogen from human serum at a concentration of 10 mg/ml in different media (EBM, EBM + VEGF, or PBS) and a crosslinking ratio of either (A, B) 200:10:1 or (C, D) 100:10:1. MVECs were cultured with EGM and seeded at a density of 2×10^4 cells/well (96-well plate). Cells-only controls were used. (ANOVA/Tukey's HSD; $p \leq 0.05$; $n = 12$).

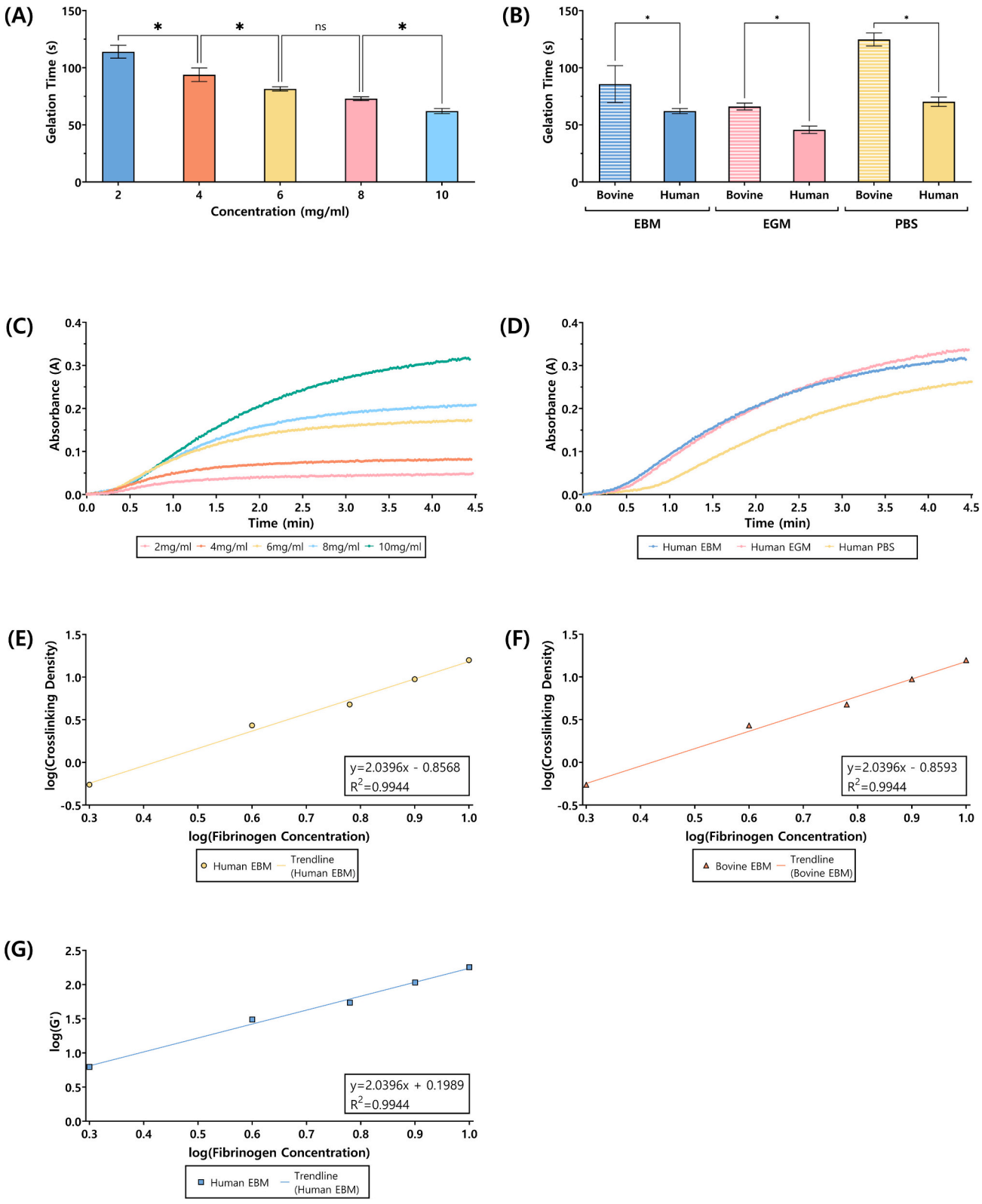

Fig. 8. Material characterisation of the 3D hydrogel constructs, depicting (A, B) gelation time, (C, D) spectrophotometry, (E-G) microrheology and crosslink density. Average gelation times (s) by hydrogel. (A) EBM hydrogels created with different concentrations of human fibrinogen. (B) Hydrogels with the same fibrinogen concentration (10 mg/ml) but using different media (EBM, EGM or PBS) or fibrinogen source (bovine or human). Error bars indicate standard deviation. (ANOVA/Tukey's HSD and 2-way ANOVA/Tukey's HSD; $p \leq 0.05$; $n = 5$). Spectrophotometry absorbance plots showing the normalised change in 340 nm light absorbance for 4.5 min. (C) EBM hydrogels created with human fibrinogen at different concentrations. (D) Human fibrin hydrogels (10 mg/ml) created with EBM, EGM or PBS. ($n = 9$). (E, F) Crosslinking density of hydrogel dependence on fibrinogen concentration and (G) storage modulus (G′) of hydrogels crafted with either (E, G) human or (F) bovine fibrinogen. From the data points, trend lines were plotted and their equation and goodness of fit (R^2) were obtained. The concentration dependence was found using the method of least squares with upper and lower-bound values.

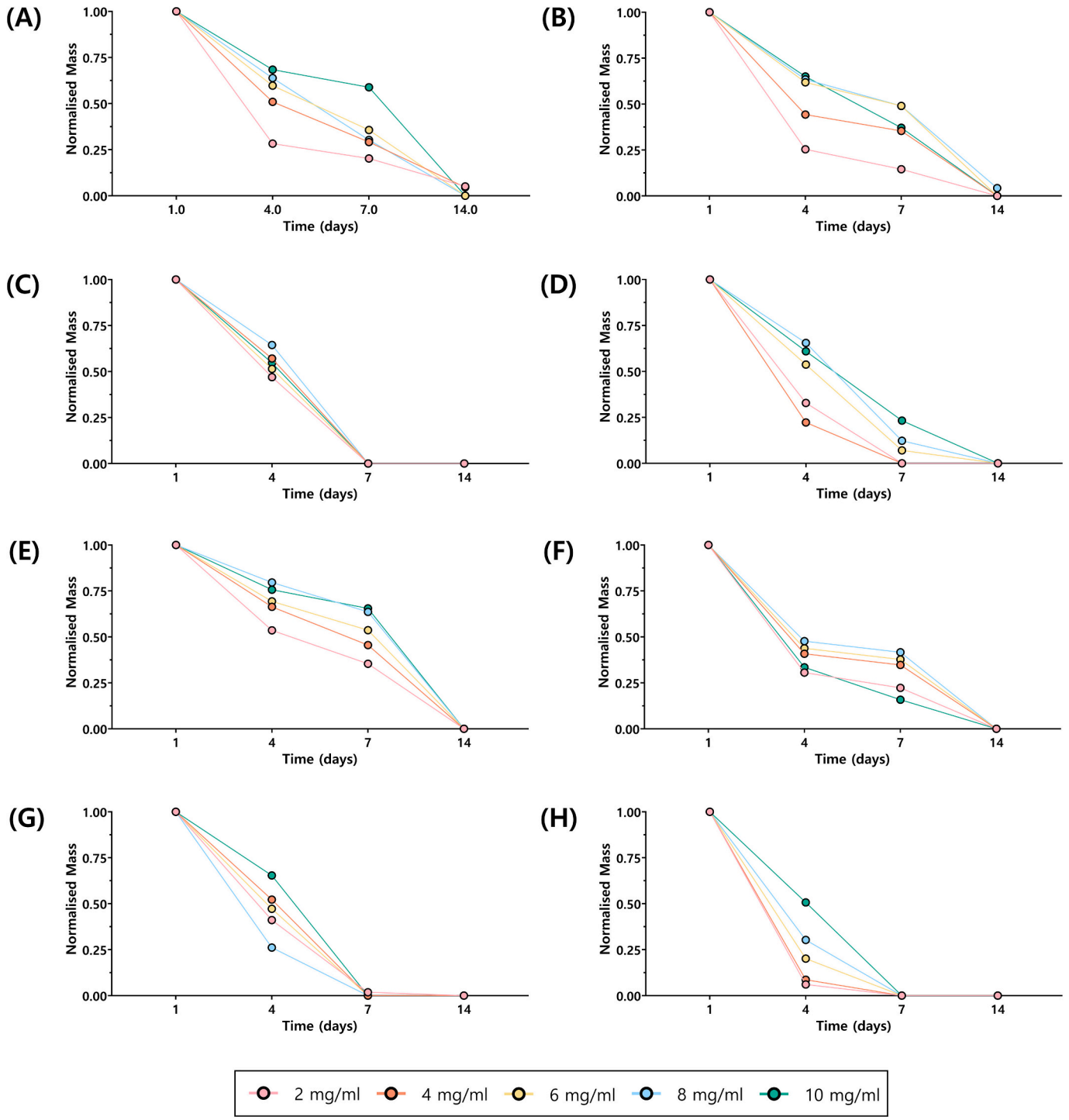

Fig. 9. Degradation of hydrogel scaffolds by fibrinogen source, concentration, and medium during a period of 14 days. Hydrogel scaffolds were created using fibrinogen from (A, C, E, G) bovine or (B, D, F, H) human serum in (A, B) EBM, (C, D) EBM + VEGF, (E, F) EGM, or (G, H) PBS. Each hydrogel scaffold was created by casting 100 μl of a hydrogel solution per well (96-well). (ANOVA/Tukey's HSD; $p \leq 0.05$; $n = 3$).

vascular network formation [65]. Gelation time is also key to ensure optimal cell distribution by balancing sufficient gelation time to allow for uniform cell distribution and avoiding cell aggregation and uneven cell densities.

Higher fibrinogen concentrations significantly reduced gelation times (Fig. 8A). For example, a five-fold increase in human fibrinogen concentration (EBM hydrogels) decreased gelation time by 1.84-fold (Fig. 8A). Additionally, gelation times were influenced by the fibrinogen source and medium. For instance, human fibrinogen hydrogels gelled slower than bovine ones at the same concentration; while EBM significantly decreases gelation times compared to PBS but significantly increases it compared to EGM when using the same medium (Fig. 8B).

The increase in fibrinogen concentration in hydrogels of the same fibrinogen source and medium results in shorter gelation times. As exemplified by EBM hydrogels with human fibrinogen, a fivefold increase in fibrinogen concentration is associated with a 1.84-fold decrease in gelation time.

Maintaining the fibrinogen concentration unchanged (10 mg/ml;

Fig. 8B), we observe that when using human fibrinogen and the same medium (EBM, EGM or PBS), gelation times decrease in comparison with hydrogels made with bovine fibrinogen. The medium also plays a role in gelation times. For instance, within the same fibrinogen concentration (10 mg/ml) and source (bovine), PBS hydrogels have significantly longer gelation times compared to EBM, which are also associated with significantly longer gelation times than EGM.

3.4.2. Spectrophotometry

Spectrophotometry provided valuable quantitative insights into hydrogel consistency and shape retention, including gelation kinetics [66] and concentration profiles [67]. Similarly to gelation times, spectrophotometry data can be used to inform hydrogel formulation to achieve uniform cell density throughout the construct. Here, we measured the normalised change in 340 nm light absorbance during 4.5 min (Fig. 8C & D) and up to 20 min (Fig. S 11).

Data from human fibrin EBM hydrogels revealed that increasing fibrinogen concentration led to greater absorbance, especially from 1 min onwards. The differences between hydrogel concentrations became more pronounced over time, with an average absorbance difference of 0.2662 between 2 and 10 mg/ml at 4.5 min (6.58-fold increase). High fibrinogen concentrations also exhibited a greater rate of change in absorbance (dA/dt), whereas lower concentrations showed a noticeably smaller rate of change, particularly after 2 min. The choice of medium also influenced absorbance. PBS consistently had lower absorbance compared with EBM or EGM hydrogels of the same concentration and fibrinogen source. Interestingly, absorbance differences between EBM and EGM hydrogels were minimal until 2.5 min, after which the rate of change increased, particularly after 5 min (Fig. S 11).

Turbidity measurements of fibrin gels provided estimates of the mass per unit length of fibrils in the hydrogel [68], allowing for approximation of fibre size and density based on the incident light wavelength measured [69]. Greater turbidity, reflected by higher absorbance, indicates a greater mass per unit length of fibrils and a denser gel structure.

Both gelation times and spectrophotometry provide insights into the polymerisation dynamics of hydrogels, which influence their microstructure and material properties. As reported by Allan [40], increasing fibrinogen concentrations enhances network development, as supported by the shortened gelation times and increased rates of absorbance with time observed here. Thus, hydrogels with higher fibrinogen concentrations were denser at any time point, aligning with Carr's findings that using higher concentrations shortens the time to reach the critical gelation point and, therefore, have a shortened gelation time [68].

Regarding network formation, the increased absorbance rate in higher fibrinogen concentrations may be attributed to an elevated monomer supply rate [40]. Since thrombin volume remained unchanged across all formulations, these results suggest that the reaction rate in these hydrogel formulations is not limited by thrombin availability.

3.4.3. Microrheology and crosslink density

Fibrinogen concentration emerged as the primary factor driving changes in the storage modulus and crosslinking density, displaying a positive relation with their logarithmic values (Fig. 8E-G). Crosslink density calculations used the following values: polymer density for fibrinogen [70]: 1395 g/cm^3; molecular weight: 340 kDa (bovine fibrinogen [70]) and 342 kDa (human fibrinogen [71]); and G' at 100 rad/s as an approximation to the plateau value.

Microrheology characterisation revealed similar findings, with fibrinogen concentration having the greatest impact, followed by the fibrinogen source. The storage modulus (G′), loss modulus (G″), complex shear modulus (G*), complex viscosity (η^*) and creep compliance 1 h after gelation were obtained for hydrogels with varying fibrinogen concentrations and hydrogels with a 10 mg/ml fibrinogen concentration of bovine or human source (Fig. S 12).

Increasing fibrinogen concentration significantly impacted the microrheological properties, leading to higher G′, G″ and complex viscosity while decreasing creep compliance. For example, at 100 rad/s, an increase in fibrinogen concentration from 2 to 10 mg/ml resulted in a 29-fold rise in G′, an 8-fold rise in G″, an 18.7-fold rise in complex viscosity, and a 27-fold reduction in creep compliance.

Hydrogels created with different media but at the same fibrinogen concentration (10 mg/ml) displayed similar trends across parameters, with some medium-dependent differences. For instance, PBS paired with human fibrinogen exhibited a lower G″ minimum compared to its bovine counterparts. EGM hydrogels displayed a slight increase (<10%) in G′, G″ and complex viscosity and a decrease in creep compliance compared to EBM hydrogels. After 24 h, PBS hydrogels were the only variation displaying statistically significant differences in the parameters: increase in G′, G″ and complex viscosity, and decrease in creep compliance.

The fibrinogen source also influenced microrheological properties, with bovine and human fibrinogen exhibiting similar trends in G*, complex viscosity, and creep compliance. However, differences were observed at extreme high and low frequencies for G′ and G″. In EBM hydrogels with the same fibrinogen concentration, bovine fibrinogen produced a slight increase in G′ (<10%), a decrease in G″, and an increase in complex viscosity and creep compliance compared to human fibrinogen. PBS hydrogels also exhibit some differences when comparing different fibrinogen sources: lower G′ and G″, higher complex viscosity, but similar creep compliance.

After 24 h, the microrheological properties of the hydrogels exhibited subtle changes. EBM hydrogels with bovine fibrinogen showed higher G′, G″ and compliance but lower viscosity compared to human fibrinogen hydrogels. Conversely, PBS hydrogels exhibited higher G' and G″ with bovine fibrinogen, but, unlike EBM hydrogels, demonstrated increased viscosity and reduced creep compliance relative to human fibrinogen.

3.4.4. Hydrogel degradation

Hydrogel scaffold degradation was monitored over 14 days (Fig. 9), with 96.67% of samples fully degrading by the end of the period. Only three bovine and one human fibrin hydrogels in EBM did not entirely degrade, but their mass significantly decreased to 1.72–13.81% of their initial values.

Data analysis tested linear, exponential, and polynomial trend lines were trialled to describe degradation patterns. The second order polynomial fit provided the highest $R2$ value across all samples, significantly outperforming linear fits. This indicates faster degradation in the initial days, followed by slower degradation rates towards the end of the period. Here, the exponential degradation curves suggest hydrolysis as the likely degradation mechanism. Further experimental work conducted at shorter intervals and with an increased number of repeats are required to confirm this.

Lower concentrations of fibrinogen generally degraded faster, with some exceptions. For instance, the 10 mg/ml human fibrinogen in EBM and in EGM degraded faster than the 6 and 8 mg/ml. Across the same fibrinogen source, hydrogels with EBM + VEGF or PBS degraded faster than those with EBM or EGM. In most cases, human fibrin hydrogels degraded slower than their bovine counterparts, particularly in EGM and PBS media.

These findings align with the literature, showing that mass, including of fibrin samples, decreases by day 7 [72]. The degradation rate is crucial for tissue engineering constructs, balancing scaffold breakdown with cell growth. Rapid degradation can lead to the loss of mechanical attachment points for cells and, consequently, impairs cell growth. On the other hand, too slow degradation can lead to cell crowding and death [39].

Our experimental results indicate that higher fibrinogen concentrations degrade more slowly. Similar findings have been reported and could be attributed to increased crosslinking density and mechanical strength, which have greater resistance to enzymatic degradation [73]. Degradation rates also vary across media, influenced by solubility,

structural integrity, β-chain crosslinking, and interaction with proteins and organic molecules [74]. As such, modifying the fibrinogen concentration and, to a lesser extent, changing the media impact the degradation rate.

These factors underscore the importance of fibrinogen's biochemical properties and crosslinking mechanisms in determining scaffold stability and degradation behaviour. Fibrinogen crosslinks with thrombin through thrombin-mediated proteolytic cleavage, forming protofibres and mature fibres that grant both biochemical and mechanical stability [75]. Therefore, the crosslinking mechanism that the fibrin hydrogels undergo enables the scaffolds to display good stability, which is paramount for long term tissue engineering applications. Our results suggest that hydrogels with higher fibrinogen concentrations in EBM, EBM + VEGF (human fibrinogen only), and EGM degrade more slowly, making them better candidates for microvasculature constructs by maintaining a stable mechanical support structure for embedded cells.

3.5. Developing a microvascular construct for long-term network integrity

Considering that fibrinogen from both bovine and human plasma source can produce 3D hydrogel scaffolds that enable endothelial network formation, human fibrinogen was selected to preserve species specificity with the cell line. Hydrogels embedded with MVECs were evaluated over 13 days (Fig. 10) to gain further insights into capillary-like network development and architecture. Embedding MVECs into 3D scaffolds supported long-term network stability and enabled shape retention for at least 13 days post-seeding (Fig. 10G), demonstrating usability well beyond the 18-24 h period of standard HUVEC-based models [28–31].

The microvascular networks were imaged and characterised over 53 h (Figs. 10A & B and S 13), showing that hydrogel constructs sustained a stable network after the first 11 h, with increasing number of segments and total network length, unlike the controls, which exhibited network degradation from 24 h onwards. Notably, network formation and disintegration occurred more rapidly in the absence of hydrogels, which could potentially suggest that both of these processes happen at an accelerated pace when there are no 3D structures supporting the endothelial networks, highlighting their role in supporting durable networks.

The trends exhibited in the number of segments and the total network length are remarkably similar, suggesting that the increasing segment count reflects network growth rather than disintegration into independent segments. At the last time point, all hydrogel constructs supported longer microvascular networks and with more segments than the controls, with one exception (2 mg/ml EBM hydrogel). This may result from the natural progression of network formation followed by fragmentation [23], as exhibited by both HUVECs and MVECs. As previously observed and further supported by the literature [23,28,29,31], HUVEC networks disintegrate towards the end of the first 24 h when unsupported by a scaffold. Similarly, MVECs undergo the same process later, leading to network breakage by day 2.

In EBM hydrogels, segment numbers stabilised after 11 h, with higher fibrinogen concentrations associated with longer networks and more segments. A similar trend was observed in EBM + VEGF hydrogels, though more clearly at 53 h. Within this group, the 10 mg/ml concentration produced the longest network and the greatest number of segments, except at 3.5 h. This suggests that this hydrogel composition is particularly well-suited for microvascular network formation and growth. Furthermore, EGM constructs exhibited more consistent behaviour across different fibrinogen concentrations, particularly within the initial 24 h, compared to EBM or EBM + VEGF hydrogels.

VEGF, known to upregulate endothelial nitric oxide synthase production, is crucial for regulating and maintaining healthy vasculature, and can aid in limiting tissue injury [76]. Additionally, VEGF has demonstrated significant protective effects, including improved endothelial preservation, survival time prolongation, and increased survival rates [77]. These findings align with the experimental results, suggesting that the use of EBM + VEGF as a medium in hydrogel constructs may enhance the long-term integrity of microvascular networks.

Longer term network characterisation (Figs. 10C & D and S 14) further highlighted the essential role of 3D scaffolds. Controls exhibited significantly lower segment numbers and shorter network lengths compared to EBM and EBM + VEGF hydrogels. EGM hydrogels, on the other hand, produced poorer results than the hydrogels created with other media. EBM and EBM + VEGF performed comparably, supporting longer networks than EGM scaffolds. For both EBM and EBM + VEGF, higher fibrinogen concentrations generally produced longer networks, though increasing concentrations beyond 6 mg/ml yielded no significant additional benefit in network architecture.

Networks were monitored for up to 13 days to assess stability (Figs. 10E & F and S 15). The controls, as expected, exhibited a noticeable decrease of network length from day 4 to day 13, likely due to insufficient mechanical support for 3D network development. While hydrogels also showed some reduction in network length, the effect was significantly less pronounced.

PBS hydrogels proved suboptimal for network preservation, as total network length remained relatively stable between days 6 and 13, but was consistently lower than other hydrogel groups. This may be attributed to the absence of specific EBM components necessary for a conducive microvascular environment, beyond the media used to culture the cell-embedded hydrogels.

Both EBM and EBM + VEGF hydrogels supported more stable MVEC networks. Despite a noticeable network length reduction from day 4 to day 6, three fibrinogen concentrations at 200:10:1 ratio of EBM hydrogels remain at similar lengths until the end of the period. Interestingly, the 6 mg/ml concentration in EBM and EBM + VEGF at 100:10:1 hydrogels showed a unique trend: an initial reduction in length followed by an increase between days 6 and 14, which was significant only in the EBM + VEGF hydrogels.

Finally, the 8 and 10 mg/ml concentrations at 100:10:1 ratio of EBM and EBM + VEGF maintained relatively stable networks up to day 7 (EBM) or day 14 (EBM + VEGF). This suggests that higher fibrinogen concentrations combined with a 200:10:1 crosslinking ratio produced the most robust networks and thus provide a more suitable 3D environment for long-term microvascular network stability.

The stability of MVEC-based constructs observed over 13 days correlates with findings that hydrogel scaffolds with optimised stiffness and biochemical cues can support endothelial functionality [87]. This is a key consideration for trauma models, where long-term observations of microvascular injury and repair processes are critical.

Based on the results, five compositions emerged as the best candidates for forming the longest networks and with the best integrity preservation at 4-, 5- and 6-days post-seeding. Interestingly, these were the highest fibrinogen concentrations in EBM (6, 8 and 10 mg/ml) and EBM + VEGF (8 and 10 mg/ml). These hydrogels shared similar architecture between them, making them the most promising candidates for developing microvasculature constructs.

It can be argued that, since EBM + VEGF hydrogels did not demonstrate significant advantages in preserving network integrity compared to EBM hydrogels, the latter may be preferable for developing 3D microvascular constructs due to their comparable performance and simpler formulation.

3.6. Impact of hydrogel composition on network architecture and material characteristics: key results

Based on the experimental results obtained in this research, a summary table (Table 2) was created to outline the impact of the different elements of the hydrogel composition — such as medium, fibrinogen concentration, source, and the fibrinogen : thrombin : $CaCl_2$ crosslinking ratio — on both material properties and network architecture.

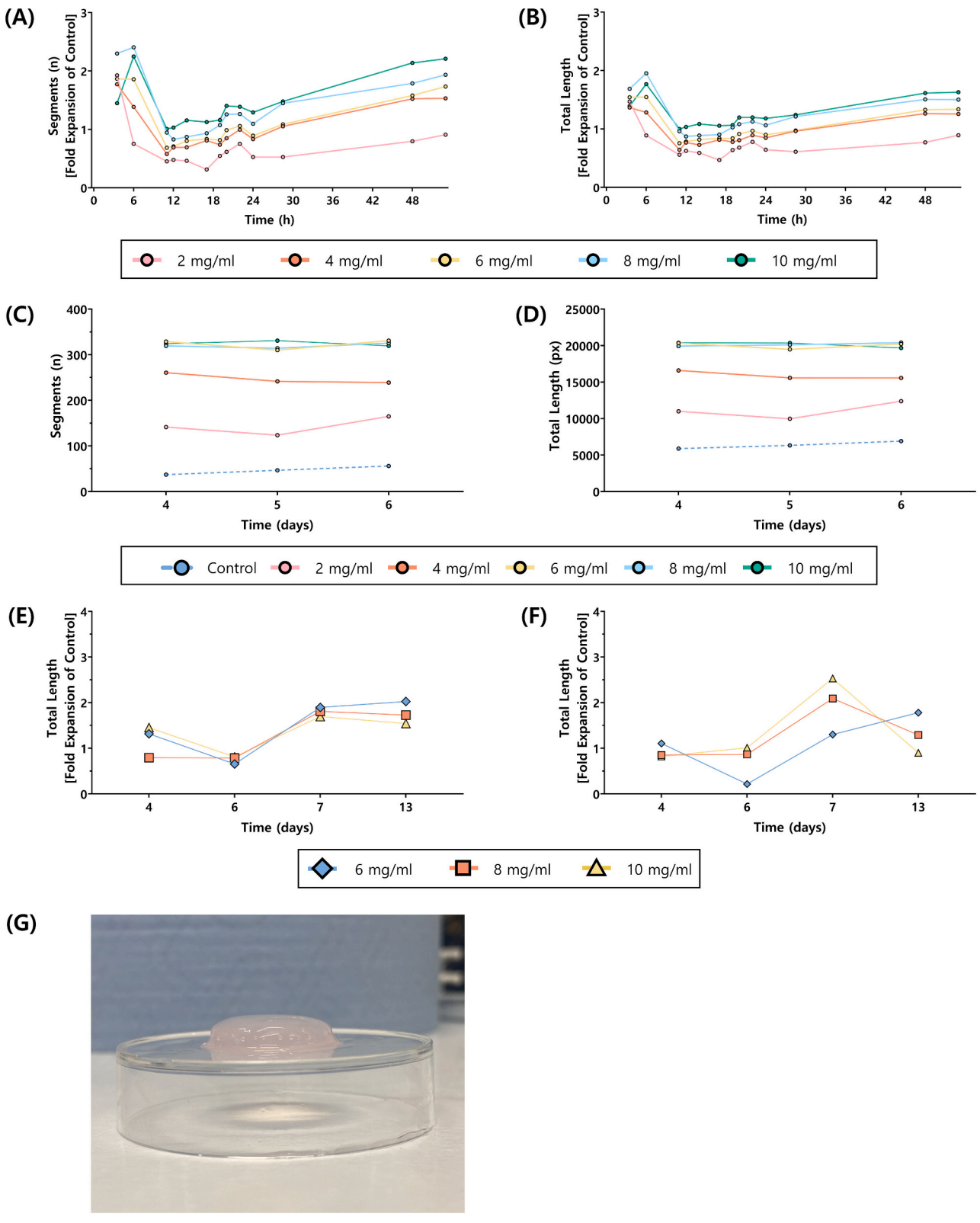

Fig. 10. Optimisation of a microvascular construct for long-term network integrity. Characterisation of MVEC networks embedded in 3D hydrogel scaffolds, quantified throughout (A, B) 53 h, (C, D) 6 days, and (E, F) 13 days depicting (A, C, E) number of segments and (B, D, F) total network length. Hydrogels were created using fibrinogen from human serum at different fibrinogen concentrations (2–10 mg/ml), media, and crosslinked at (A-E) 200:10:1 or (F) 100:10:1 ratio (fibrinogen : thrombin : $CaCl_2$). The data from EBM hydrogels is shown here, while the data related to EBM + VEGF and EGM hydrogels is available in Figs. S 13, S 14 & S 15. MVECs were cultured with EGM until hydrogel casting, after which they were cultured with EBM. Cells were seeded at a density of 1.5×10^4 cells/well (48-well plate); (C, D) 5.25×10^4 cells/well (24-well plate); or (E, F) 2×10^4 cells/well (96-well plate). Cells-only controls were used. (A, B) (ANOVA/Tukey's HSD; $p \leq 0.05$; $n = 30$); (C, D) (ANOVA/Tukey's HSD; $p \leq 0.05$; seven random images per sample, $n = 15$); (E, F) (ANOVA/Dunnett; $p \leq 0.05$; $n = 6$). (G) Photograph of 3D construct captured at 13 days after seeding. Here shown is an EBM hydrogel created with human fibrinogen at a concentration of 10 mg/ml and crosslinked at a ratio of 200:10:1 (fibrinogen : thrombin : $CaCl_2$).

Table 2
Summary of the impact on microvascular endothelial cell (MVEC) network architecture and material characteristics of variations in the hydrogel composition.

Factor	Impact on Network Architecture	Impact on Material Characterisation
Medium	• EBM vs. MES/*NaCl*: — Longer networks. — More segments, branches and junctions. — Higher branching interval. — Better network integrity at 3- and 4-days post-seeding. • EBM vs. EGM: — Greater total network length. — EBM vs. EBM + VEGF and PBS. — Less variability in total network length across ratios and fibrinogen concentrations. • EBM & EBM + VEGF vs. EGM: — More segments. — Greater total network length at 4-, 5- and 6-days post-seeding. • EBM & EBM + VEGF: — When paired with high fibrinogen concentrations, can preserve network integrity for up to 13 days post-seeding.	• PBS vs. EBM: — Longer gelation times. — Lower absorbance (in human fibrin hydrogels). — Faster degradation. • EBM vs. EGM: — Longer gelation times. — Greater absorbance of human fibrin hydrogels (< 3 min). — Hydrogels are slightly softer, more flexible, more easily deformable, and have a lower resistance to shear forces. • PBS vs. EGM: — Lower absorbance (in human fibrin hydrogels). — Faster degradation. • PBS: — Faster gelation. — Hydrogels are more viscous. • EBM + VEGF: — Faster degradation than EBM or EGM hydrogels.
Fibrinogen Concentration	• Higher fibrinogen concentration: — Greater total network length.	• Higher fibrinogen concentration: — Faster rate of fibrin network development: a 5× increase in concentration leads to 1.84× decrease in gelation time. — Denser hydrogels. — The deformation response is stiffer and more elastic: 5× increase in concentration leads to a 29× increase in G′. — Slower degradation rate.
Fibrinogen Source	• Both bovine and human fibrinogen enable the formation of endothelial networks. • Pairing human fibrinogen with human cells permits species compatibility between the construct components, which can lead to a more physiologically relevant construct with enhanced biocompatibility	• Bovine vs. Human Fibrinogen: — Longer gelation times. — Faster degradation. — Hydrogels exhibit similar microrheology patterns, except for G′ and G″ at extreme high and extreme low frequencies. — Paired with PBS, results in less rigid and more viscous hydrogels. — Paired with EBM, has enhanced mechanical stability and greater strength.
Crosslinking Ratio (Fibrinogen : Thrombin : $CaCl_2$)	• 200:10:1 vs. 100:10:1 ratio: — Greater number of segments. — Longer networks.	• 200:10:1 vs. 100:10:1 ratio: — Slower gelation.

4. Conclusion

The microvasculature construct developed here aims to provide a more physiologically relevant model for trauma research, featuring a 3D structure, microvascular cells, and long-term endothelial network integrity. MVECs can create more durable endothelial networks than HUVECs, which are often considered the gold standard. When embedded in a 3D hydrogel construct, MVECs can form extensive and complex networks that are stable for a prolonged period of time, making these constructs a valuable tool for traumatic injury research.

Modifications to the hydrogel composition — specifically the source and concentration of fibrinogen, the crosslinking ratio, and the medium — affect the material properties of the scaffold, the network architecture and its long-term integrity. Through optimisation, it was found that hydrogels using human serum-derived fibrinogen at higher concentrations (>6 mg/ml), crosslinked at a ratio of 200:10:1 (fibrinogen : thrombin : $CaCl_2$), and with EBM as the medium, are particularly well suited for maintaining the stability of microvascular endothelial networks. In the long term, these compositions exhibited slower degradation rates, shorter gelation times, enabled longer networks with more segments and branches, and maintained the network integrity for at least 13 days post-seeding.

Further work, for instance, immunofluorescence staining of the microvasculature constructs will be beneficial to further validate the microvascular phenotype through, for example, CD36, as well as advanced characterisation of 3D vascular networks using confocal microscopy. It would also be useful to monitor the evolution of material properties during gelation as this could help gain a further understanding of the mechanical properties of the hydrogel scaffolds as they are formed. Also, material characterisation of cell-embedded hydrogels would be valuable to assess the impact of cell loading and microvascular network formation on scaffold properties.

As for the applications of the 3D hydrogel construct embedded with a microvascular endothelial network developed here, future work will use this to study a range of traumatic injuries. In the long term, this microvasculature construct could have applications beyond contributing to a further understanding of the mechanisms of trauma; for instance, by serving as a platform for testing potential therapeutics that target not only tissue repair and regeneration, but also help mitigate traumatic injury damage.

AbbreviationsThe following abbreviations are used in this manuscript:

ANOVA	Analysis of Variance
COVID-19	Coronavirus Disease
EBM	Endothelial Basal Cell Medium
EBM + VEGF	Endothelial Basal Cell Medium Supplemented with VEGF
ECM	Extracellular Matrix
EGM	Endothelial Growth Cell Medium
FBS	Foetal Bovine Serum
HSD	Honest Significant Difference
HUVECs	Human Umbilical Vein Endothelial Cells
LSD	Least Significant Difference
MVECs	Microvascular Endothelial Cells
PBS	Phosphate-Buffered Saline
VEGF	Vascular Endothelial Growth Factor

CRediT authorship contribution statement

Carla Verónica Fuenteslópez: Writing – review & editing, Writing – original draft, Visualization, Validation, Project administration, Methodology, Investigation, Funding acquisition, Formal analysis, Conceptualization. **Mariella Papapavlou:** Writing – review & editing, Investigation, Formal analysis. **Mark S. Thompson:** Writing – review & editing, Supervision, Resources, Funding acquisition. **Hua Ye:** Writing – review & editing, Supervision, Resources, Project administration, Funding acquisition, Conceptualization.

Declaration of competing interest

The authors declare that they have no known competing financial interests or personal relationships that could have appeared to influence the work reported in this paper.

Acknowledgements

This research was funded by *Consejo Nacional de Ciencia y Tecnología* (CONACYT) as part of the fellowship *Becas CONACYT para estudios de Doctorado en el Extranjero* awarded to C.V.F. [grant number 2019-000021-01EXTF-00672], and by the Bank of Mexico through *Fondo para el Desarrollo de Recursos Humanos* (FIDERH) awarded to C.V.F. [grant number 1911110682]. C.V.F. is a recipient of the Foundation Grant kindly awarded by Funds for Women Graduates (FfWG) for living expenses.

HUVECs and MVECs were generous gifts, kindly provided by Professor Sarah De Val & Dr Susann Bruche (Department of Physiology, Anatomy and Genetics, University of Oxford), and by Dr Helen Sheldon (Department of Oncology, University of Oxford), respectively.

Appendix A. Supplementary data

Supplementary data to this article can be found online at https://doi.org/10.1016/j.bioadv.2025.214310.

Data availability

The data presented in this research are available upon request from the corresponding author.

References

[1] Akinori Osuka, Hiroshi Ogura, Masashi Ueyama, Takeshi Shimazu, James A. Lederer, Immune response to traumatic injury: harmony and discordance of immune system homeostasis, Acute Medicine & Surgery 1 (2014) 63–69.
[2] Herman R. Holtslag, Eduard F. Van Beeck, Rob A. Lichtveld, Loek Ph. Leenen, Eline Lindeman, Chris Van Der Werken, Individual and population burdens of major trauma in the Netherlands, Bull. World Health Organ. 86 (2008) 111–117.
[3] K.D. Schaser, B. Vollmar, M.D. Menger, L. Schewior, S.N. Kroppenstedt, M. Raschke, A.S. Lubbe, N.E. Haas, T. Mittlmeier, In vivo analysis of microcirculation following closed soft-tissue injury, J. Orthop. Res. 17 (1999) 678–685.
[4] Birte Weber, Ina Lackner, Melanie Haffner-Luntzer, Annette Palmer, Jochen Pressmar, Karin Scharffetter-Kochanek, Bernd Knöll, Hubert Schrezenemeier, Borna Relja, Miriam Kalbitz, Modeling trauma in rats: similarities to humans and potential pitfalls to consider, J. Transl. Med. 17 (2019) 305.
[5] Janaka Senarathna, Arvind P. Pathak, Visualizing the microcirculation, Microcirculation 29 (2022) e12785.
[6] Kirsty A. Roberts, Liam Colley, Thomas A. Agbaedeng, Georgina M. Ellison-Hughes, Mark D. Ross, Vascular manifestations of covid-19 — thromboembolism and microvascular dysfunction, Frontiers in Cardiovascular Medicine 7 (2020) 10.
[7] Douglas Hanahan, Hallmarks of cancer: new dimensions, Cancer Discov. 12 (2022) 31–46.
[8] Danielle K. Sandsmark, Asma Bashir, Cheryl L. Wellington, R. Diaz-Arrastia, Cerebral microvascular injury: a potentially treatable endophenotype of traumatic brain injury-induced neurodegeneration, Neuron 103 (2019) 367–379.
[9] Klemens Horst, Johannes Greven, Hannah Lüken, Qiao Zhi, Roman Pfeifer, Tim P. Simon, Borna Relja, Ingo Marzi, Hans Christoph Pape, Frank Hildebrand, Trauma severity and its impact on local inflammation in extremity injury—insights from a combined trauma model in pigs, Front. Immunol. 10 (2020) 1.
[10] Kristina Funk, Nina Scheerer, Rabea Verhaegh, Carolin Pütter, Joachim Fandrey, Herbert De Groot, Severe blunt muscle trauma in rats: only marginal hypoxia in the injured area, PLoS One 9 (2014) 10.
[11] Ping Xia, Yongxiang Luo, Vascularization in tissue engineering: the architecture cues of pores in scaffolds, J Biomed Mater Res B Appl Biomater 110 (5) (2022) 1206–1214.
[12] Mani T. Valarmathi, John W. Fuseler, Jay D. Potts, Jeffrey M. Davis, Robert L. Price, Functional tissue engineering: a prevascularized cardiac muscle construct for validating human mesenchymal stem cells engraftment potential in vitro, Tissue Engineering - Part A 24 (2018) 157–185.
[13] Radman Mazloomnejad, Amirhesam Babajani, Mohammadreza Kasravi, Armin Ahmadi, Siavash Shariatzadeh, Soheyl Bahrami, Hassan Niknejad, Angiogenesis and re-endothelialization in decellularized scaffolds: recent advances and current challenges in tissue engineering, Front. Bioeng. Biotechnol. 11 (2023).
[14] Jordan A. Whisler, Michelle B. Chen, Roger D. Kamm, Control of perfusable microvascular network morphology using a multiculture microfluidic system, Tissue Engineering: Part C 20 (2014) 543–552.
[15] Adeeba Shakeel, Peter R. Corridon, Mitigating challenges and expanding the future of vascular tissue engineering—are we there yet? Front. Physiol. 13 (2022) 1.
[16] W.H. Zimmermann, C. Fink, D. Kralisch, U. Remmers, J. Weil, T. Eschenhagen, Three-dimensional engineered heart tissue from neonatal rat cardiac myocytes, Biotechnol. Bioeng. 68 (2000) 106–114.
[17] Arinola O. Lampejo, Hu Nien Wen, Daniela Lucas, Banks M. Lomel, Christian M. Nguyen, Carmen C. Dominguez, Bing Ren, Yong Huang, Walter L. Murfee, A challenge for engineering biomimetic microvascular models: how do we incorporate the physiology? Front. Bioeng. Biotechnol. 10 (2022) 6.
[18] Roland Kaunas, Hojin Kang, Kayla J. Bayless, Synergistic regulation of angiogenic sprouting by biochemical factors and wall shear stress, Cell. Mol. Bioeng. 4 (2011) 547–559.
[19] Bing Ren, Kaidong Song, Anil Reddy Sanikommu, Yejun Chai, Matthew A. Longmire, Wenxuan Chai, Walter Lee Murfee, Yong Huang, Study of sacrificial ink-assisted embedded printing for 3d perfusable channel creation for biomedical applications, Appl. Phys. Rev. 9 (2022) 3.
[20] Marco Campisi, Yoojin Shin, Tatsuya Osaki, Cynthia Hajal, Valeria Chiono, Roger D. Kamm, 3d self-organized microvascular model of the human blood-brain barrier with endothelial cells, pericytes and astrocytes, Biomaterials 180 (2018) 117–129.
[21] Haoxiang Chen, Yanxiang Cheng, Xiaocheng Wang, Jian Wang, Xuelei Shi, Xinghuan Li, Weihong Tan, Zhikai Tan, 3d printed in vitro tumor tissue model of colorectal cancer, Theranostics 10 (2020) 12127–12143.
[22] Yu Yi Cao, Liangliang Liu Gong, Yiwei Zhou, Xin Fang, Cao Zhang, Yining Li, Juan Li, The use of human umbilical vein endothelial cells (huvecs) as an in vitro model to assess the toxicity of nanoparticles to endothelium: a review, J. Appl. Toxicol. 37 (2017) 1359–1369.
[23] Diana J. Medina-Leyte, Mayra Domínguez-Pérez, Ingrid Mercado, María T. Villarreal-Molina, Leonor Jacobo-Albavera, Use of human umbilical vein endothelial cells (huvec) as a model to study cardiovascular disease: a review, Appl. Sci. 10 (2020) 938.
[24] Ramkumar Tiruvannamalai Annamalai, Ana Y. Rioja, Andrew J. Putnam, Jan P. Stegemann, Vascular network formation by human microvascular endothelial cells in modular fibrin microtissues, ACS Biomaterials Science and Engineering 2 (2016) 1914–1925.
[25] Ievgeniia Kocherova, Artur Bryja, Paul Mozdziak, Ana Angelova Volponi, Marta Dyszkiewicz-Konwińska, Hanna Piotrowska-Kempisty, Paweł Antosik, Dorota Bukowska, Małgorzata Bruska, Dariusz Iżycki, Maciej Zabel, Michał Nowicki, Bartosz Kempisty, Human umbilical vein endothelial cells (huvecs) co-culture with osteogenic cells: from molecular communication to engineering prevascularised bone grafts, J. Clin. Med. 8 (2019) 1602.
[26] Rebecca G. Bagley, Jennifer Walter-Yohrling, Xiaohong Cao, William Weber, Betsy Simons, Brian P. Cook, Scott D. Chartrand, Clarence Wang, Stephen L. Madden, Beverly A. Teicher, Endothelial precursor cells as a model of tumor endothelium: characterization and comparison with mature endothelial cells, Cancer Res. 63 (2003) 5866–5873.

[27] Chandran S. Abhinand, Josephine Galipon, Masaru Mori, Poornima Ramesh, Thottethodi Subrahmanya Keshava Prasad, Rajesh Raju, Perumana R. Sudhakaran, Masaru Tomita, Temporal phosphoproteomic analysis of vegf-a signaling in huvecs: an insight into early signaling events associated with angiogenesis, Journal of Cell Communication and Signaling 17 (2023) 1067.

[28] K.L. DeCicco-Skinner, G.H. Henry, C. Cataisson, T. Tabib, J.C. Gwilliam, N. J. Watson, E.M. Bullwinkle, L. Falkenburg, R.C. O'Neill, A. Morin, J.S. Wiest, Endothelial cell tube formation assay for the in vitro study of angiogenesis, J. Vis. Exp. 91 (2014 Sep 1) e51312, https://doi.org/10.3791/51312. PMID: 25225985; PMCID: PMC4540586.

[29] Xu Lu, Jianjun Zhou, Jingyu Liu, Yong Liu, Lei Wang, Ruiwei Jiang, Zhenyu Diao, Guijun Yan, Bruno Pèault, Haixiang Sun, Lijun Ding, Different angiogenic potentials of mesenchymal stem cells derived from umbilical artery, umbilical vein, and Wharton's jelly, Stem Cells Int. 2017 (2017) 3175748.

[30] Ryoji Eguchi, Hirotaka Naitou, Kazuhiro Kunimasa, Rie Ayuzawa, Yoshihiro Fujimori, Norio Ohashi, Kazuhiko Kaji, Toshiro Ohta, Proteomic analysis of hypoxia-induced tube breakdown of an in vitro capillary model composed of huvecs: potential role of p38-regulated reduction of hsp27, Proteomics 8 (2008) 2897–2906.

[31] Mary Kelley, Sara Fierstein, Laura Purkey, Kathleen DeCicco-Skinner, Endothelial cell tube formation assay: an in vitro model for angiogenesis, Methods Mol. Biol. 2475 (2022) 187–196.

[32] James E.N. Jonkman, Judith A. Cathcart, Xu Feng, Miria E. Bartolini, Jennifer E. Amon, Katarzyna M. Stevens, Pina Colarusso, An introduction to the wound healing assay using live-cell microscopy, Cell Adhes. Migr. 8 (2014) 440–451.

[33] Alejandra Suarez-Arnedo, Felipe Torres Figueroa, Camila Clavijo, Pablo Arbeláez, Juan C. Cruz, Carolina Muñoz-Camargo, An imageJ plugin for the high throughput image analysis of in vitro scratch wound healing assays, PLoS One 15 (2020).

[34] Gilles Carpentier, Sarah Berndt, Ségolène Ferratge, Wayne Rasband, Muriel Cuendet, Georges Uzan, Patricia Albanese, Angiogenesis analyzer for imageJ — a comparative morphometric analysis of "endothelial tube formation assay" and "fibrin bead assay", Sci. Rep. 10 (2020) 1–13.

[35] Lu Mei, Zheng Gang Zhang, Michael Chopp, Analysis of cerebral microvascular architecture—application to cortical and subcortical vessels in rat brain, J. Neurosci. Methods 138 (2004) 81–87.

[36] M.A. Konerding, E. Fait, A. Gaumann, 3d microvascular architecture of pre-cancerous lesions and invasive carcinomas of the colon, Br. J. Cancer 84 (2001) 1354–1362.

[37] Paula K. Yu, Chandrakumar Balaratnasingam, Stephen J. Cringle, Ian L. Mcallister, Jan Provis, Yu Dao-Yi, Microstructure and network organization of the microvasculature in the human macula, Invest. Ophthalmol. Vis. Sci. 51 (2010) 6735–6743.

[38] Jonathan Evrard, Romain Siriez, Laure Morimont, Pauline Thémans, Julie Laloy, Céline Bouvy, Damien Gheldof, François Mullier, Jean Michel Dogné, Jonathan Douxfils, Optimal wavelength for the clot waveform analysis: determination of the best resolution with minimal interference of the reagents, Int. J. Lab. Hematol. 41 (2019) 316–324.

[39] E. Sproul, S. Nandi, A. Brown, Fibrin Biomaterials for Tissue Regeneration and Repair, Woodhead Publishing, 2018, pp. 151–173.

[40] Peter Allan, Microrheology of Fibrin Clots (PhD thesis), The University of Leeds, 2012.

[41] Andrés Montero, Cristina Quílez, Leticia Valencia, Paula Girón, José Luis Jorcano, Diego Velasco, Effect of fibrin concentration on the in vitro production of dermo-epidermal equivalents, Int. J. Mol. Sci. 22 (2021) 6746.

[42] P. Patrizia Mangione, Guglielmo Verona, Alessandra Corazza, Julien Marcoux, Diana Canetti, Sofia Giorgetti, Sara Raimondi, Monica Stoppini, Marilena Esposito, Annalisa Relini, Claudio Canale, Maurizia Valli, Loredana Marchese, Giulia Faravelli, Laura Obici, Philip N. Hawkins, Graham W. Taylor, Julian D. Gillmore, Mark B. Pepys, Vittorio Bellotti, Plasminogen activation triggers transthyretin amyloidogenesis in vitro, J. Biol. Chem. 293 (2018) 14192.

[43] Sónia Gonçalves, Nuno C. Santos, J. Martins-Silva, Carlota Saldanha, Fluorescence spectroscopy evaluation of fibrinogen–estradiol binding, J. Photochem. Photobiol. B Biol. 86 (2007) 170–176.

[44] Katie M. Weigandt, Nathan White, Dominic Chung, Erica Ellingson, Yi Wang, Fu Xiaoyun, Danilo C. Pozzo, Fibrin clot structure and mechanics associated with specific oxidation of methionine residues in fibrinogen, Biophys. J. 103 (2012) 2399–2407.

[45] Tianhong Chen, Quantifying Polymer Crosslinking Density Using Rheology and Dma, 2020.

[46] Johannes Schindelin, Ignacio Arganda-Carreras, Erwin Frise, Verena Kaynig, Mark Longair, Tobias Pietzsch, Stephan Preibisch, Curtis Rueden, Stephan Saalfeld, Benjamin Schmid, Jean Yves Tinevez, Daniel James White, Volker Hartenstein, Kevin Eliceiri, Pavel Tomancak, Albert Cardona, Fiji: an open-source platform for biological-image analysis, Nat. Methods 9 (2012) 676–682.

[47] Carla V. Fuenteslópez, Mark S. Thompson, Hua Ye, Development and optimisation of hydrogel scaffolds for microvascular network formation, Bioengineering 10 (2023) 964.

[48] S. Patan, Vasculogenesis and angiogenesis as mechanisms of vascular network formation, growth and remodeling, J. Neuro-Oncol. 50 (2000) 1–15.

[49] A.F. Karamysheva, Mechanisms of angiogenesis, Biochem. Mosc. 73 (2008) 751–762.

[50] Matthew E. Kutcher, Ira M. Herman, The pericyte: cellular regulator of microvascular blood flow, Microvasc. Res. 77 (2009) 235–246.

[51] A. Bonnefoy, J. Harsfalvi, G. Pfliegler, F. Fauvel-Lafève, C. Legrand, The subendothelium of the hmec-1 cell line supports thrombus formation in the absence of von willebrand factor and collagen types i, iii and vi, Thromb. Haemost. 85 (2001) 552–559.

[52] Mei Peng, Mengyuan Yang, Yiling Ding, Yu Ling, Yali Deng, Weisi Lai, Hu. Yun, Mechanism of endogenous digitalis-like factor-induced vascular endothelial cell damage in patients with severe preeclampsia, Int. J. Mol. Med. 41 (2018) 985–994.

[53] Jin Young Lin, Kai Yin Lo, Yung Shin Sun, Effects of substrate-coating materials on the wound-healing process, Materials 12 (2019) 2775.

[54] Xiaoyu Zhang, Xiaoning Kang, Lijun Jin, Jie Bai, Wei Liu, Zunyi Wang, Stimulation of wound healing using bioinspired hydrogels with basic fibroblast growth factor (bfgf), Int. J. Nanomedicine 13 (2018) 3897.

[55] Zahra Sayyar, Gholam Reza Mahdavinia, Alireza Khataee, Dual-drug (curcumin/ciprofloxacin) loading and release from chitosan-based hydrogels embedded with magnetic montmorillonite/hyaluronic acid for enhancing wound healing, J. Biol. Eng. 17 (2023) 66.

[56] Donghyun Paul Jeong, Eva Hall, Erin Neu, Donny Hanjaya-Putra, Podoplanin is responsible for the distinct blood and lymphatic capillaries, Cell. Mol. Bioeng. 15 (2022) 467.

[57] Kaitlyn R. Ammann, Katrina J. DeCook, Phat L. Tran, Valerie M. Merkle, Pak K. Wong, Marvin J. Slepian, Collective cell migration of smooth muscle and endothelial cells: impact of injury versus non-injury stimuli, J. Biol. Eng. 9 (2015) 1–15.

[58] Andrew D. Doyle, Nicole Carvajal, Albert Jin, Kazue Matsumoto, Kenneth M. Yamada, Local 3d matrix microenvironment regulates cell migration through spatiotemporal dynamics of contractility-dependent adhesions, Nat. Commun. 6 (2015) 1–15.

[59] Anita Akbarzadeh Solbu, David Caballero, Spyridon Damigos, Subhas C. Kundu, Rui L. Reis, Øyvind Halaas, Aman S. Chahal, Berit L. Strand, Assessing cell migration in hydrogels: an overview of relevant materials and methods, Materials Today Bio 18 (2023) 100537.

[60] Vaibhav Sharma, Nimesha Patel, Julian F. Dye, Lilian Hook, Chris Mason, Elena García-Gareta, Albumin removal from human fibrinogen preparations for manufacturing human fibrin-based biomaterials, Biochimie Open 1 (2015) 6–10.

[61] Lorel M. Colgin, Roger R. Reddel, Telomere maintenance mechanisms and cellular immortalization, Curr. Opin. Genet. Dev. 9 (1999) 97–103.

[62] E.W. Ades, F.J. Candal, R.A. Swerlick, V.G. George, S. Summers, D.C. Bosse, T. J. Lawley, Hmec-1: establishment of an immortalized human microvascular endothelial cell line, J. Invest. Dermatol. 99 (1992) 683–690.

[63] Hyun Wook Kang, Sang Jin Lee, In Kap Ko, Carlos Kengla, James J. Yoo, Anthony Atala, A 3d bioprinting system to produce human-scale tissue constructs with structural integrity, Nat. Biotechnol. 34 (2016) 312–319.

[64] Sanskrita Das, Falguni Pati, Yeong Jin Choi, Girdhari Rijal, Jin Hyung Shim, Sung Won Kim, Alok R. Ray, Dong Woo Cho, Sourabh Ghosh, Bioprintable, cell-laden silk fibroin–gelatin hydrogel supporting multilineage differentiation of stem cells for fabrication of three-dimensional tissue constructs, Acta Biomater. 11 (2015) 233–246.

[65] Kuan Chih Kuo, Ruei Zeng Lin, Han Wen Tien, Wu Pei Yun, Yen Cheng Li, Juan M. Melero-Martin, Ying Chieh Chen, Bioengineering vascularized tissue constructs using an injectable cell-laden enzymatically crosslinked collagen hydrogel derived from dermal extracellular matrix, Acta Biomater. 27 (2015) 151–166.

[66] Sindre H. Bjørnøy, Stefan Mandaric, David C. Bassett, Andreas K.O. Åslund, Seniz Ucar, Jens Petter Andreassen, Berit L. Strand, Pawel Sikorski, Gelling kinetics and in situ mineralization of alginate hydrogels: a correlative spatiotemporal characterization toolbox, Acta Biomater. 44 (2016) 243–253.

[67] Erik N. Dunmire, Audra M. Plenys, David F. Katz, Spectrophotometric analysis of molecular transport in gels, J. Control. Release 57 (2) (1999) 127–140.

[68] Marcus E. Carr, Don A. Gabriel, The effect of dextran 70 on the structure of plasma-derived fibrin gels, J. Lab. Clin. Med. 96 (1980) 985–993.

[69] Fabio Ferri, Gabriele Re Calegari, Matteo Molteni, Barbara Cardinali, Davide Magatti, Mattia Rocco, Size and density of fibers in fibrin and other filamentous networks from turbidimetry: beyond a revisited carr-hermans method, accounting for fractality and porosity, Macromolecules 48 (2015) 5423–5432.

[70] C. Yeromonahos, B. Polack, F. Caton, Nanostructure of the fibrin clot, Biophys. J. 99 (2010) 2018–2027.

[71] P. Fantl, H.A. Ward, Molecular weight of human fibrinogen derived from phosphorus determinations, Biochem. J. 96 (1965) 886–889.

[72] Leo Benning, Ludwig Gutzweiler, Kevin Tröndle, Julian Riba, Roland Zengerle, Peter Koltay, G. Stefan Zimmermann, Björn Stark, Günter Finkenzeller, Assessment of hydrogels for bioprinting of endothelial cells, Journal of Biomedical Materials Research - Part A 106 (4) (2018) 935–947.

[73] Jin Su Kim, Tae Hyung Kim, Dong Lim Kang, Song Yeon Baek, Yura Lee, Yong Gon Koh, Yong Il Kim, Chondrogenic differentiation of human ascs by stiffness control in 3d fibrin hydrogel, Biochem. Biophys. Res. Commun. 522 (2020) 213–219.

[74] Charles W. Francis, Victor J. Marder, A molecular model of plasmic degradation of crosslinked fibrin, Semin. Thromb. Hemost. 8 (1982) 25–35.

[75] Marlien Pieters, Alisa S. Wolberg, S. Alisa Wolberg, Fibrinogen and fibrin: an illustrated review, Res. Pract. Thromb. Haemost. 3 (2019) 161–172.

[76] N. Tran, T. Garcia, M. Aniqa, S. Ali, A. Ally, S.M. Nauli, Endothelial nitric oxide synthase (enos) and the cardiovascular system: in physiology and in disease states, Am. J. Biomed. Sci. Res. 15 (2022) 153–177.

[77] Barry Campbell, Craig Chuhran, Allan M. Lefer, Vascular endothelial growth factor attenuates trauma-induced injury in rats, Br. J. Pharmacol. 129 (2000) 71–76.

[78] Z. Abdullah, U. Bayraktutan, NADPH oxidase mediates TNF-α-evoked in vitro brain barrier dysfunction: roles of apoptosis and time, Mol. Cell. Neurosci. 61 (Jul 1 2014) 72–84.

[79] M.S. Kluger, P.R. Clark, G. Tellides, V. Gerke, J.S. Pober, Claudin-5 controls intercellular barriers of human dermal microvascular but not human umbilical vein endothelial cells, Arteriosclerosis, Thrombosis, and Vascular Biology [Internet] 33 (3) (Mar 2013) 489. Available from: https://pmc.ncbi.nlm.nih.gov/articles/PMC3655806/ (cited 2025 Jan 17).

[80] F. Akther, P. Little, Z. Li, N.T. Nguyen, H.T. Ta, Hydrogels as artificial matrices for cell seeding in microfluidic devices, RSC Adv. [Internet] 10 (71) (Nov 24 2020) 43682. Available from: https://pmc.ncbi.nlm.nih.gov/articles/PMC9058401/ (cited 2025 Jan 17).

[81] J. Ballester-Beltrán, M. Lebourg, M. Salmerón-Sánchez, Dorsal and ventral stimuli in sandwich-like microenvironments. Effect on cell differentiation, Biotechnology and Bioengineering [Internet]. 110 (11) (Nov 1 2013) 3048–3058. Available from: https://onlinelibrary.wiley.com/doi/full/10.1002/bit.24972 (cited 2025 Jan 17).

[82] J.R. Libby, H. Royce, S.R. Walker, L. Li, The role of extracellular matrix in angiogenesis: beyond adhesion and structure, Biomaterials and Biosystems. 15 (Sep 1 2024) 100097.

[83] J. Song, S. Gerecht, Hydrogels to recapture extracellular matrix cues that regulate vascularization, Arteriosclerosis, Thrombosis, and Vascular Biology [Internet]. 43 (8) (Aug 1 2023) E291–E302. Available from: https://www.ahajournals.org/doi/10.1161/ATVBAHA.122.318235 (cited 2025 Jan 17).

[84] G.J. Pahapale, J. Tao, M. Nikolic, S. Gao, G. Scarcelli, S.X. Sun, et al., Directing multicellular organization by varying the aspect ratio of soft hydrogel microwells, Adv. Sci. [Internet] 9 (17) (Jun 1 2022) 2104649. Available from: https://onlinelibrary.wiley.com/doi/full/10.1002/advs.202104649 (cited 2025 Jan 17).

[85] W. Wang, E.M. Lollis, F. Bordeleau, C.A. Reinhart-King, Matrix stiffness regulates vascular integrity through focal adhesion kinase activity, FASEB Journal: Official Publication of the Federation of American Societies for Experimental Biology [Internet] 33 (1) (Jan 1 2019) 1199–1208. Available from: https://pubmed.ncbi.nlm.nih.gov/30102569/ (cited 2025 Jan 17).

[86] F. Bordeleau, B.N. Mason, E.M. Lollis, M. Mazzola, M.R. Zanotelli, S. Somasegar, et al., Matrix stiffening promotes a tumor vasculature phenotype, Proc. Natl. Acad. Sci. U.S.A. [Internet] 114 (3) (Jan 17 2017) 492–497. Available from: https://pmc.ncbi.nlm.nih.gov/articles/PMC5255592/ (cited 2025 Jan 17).

[87] P. Lu, D. Ruan, M. Huang, M. Tian, K. Zhu, Z. Gan, et al., Harnessing the potential of hydrogels for advanced therapeutic applications: current achievements and future directions, Signal Transduction and Targeted Therapy 9 (1) (Jul 1 2024) 1–66. Available from: https://www.nature.com/articles/s41392-024-01852-x (cited 2025 Jan 17).